Connecting $(g-2)_\mu$ to neutrino mass in the extended neutrinophilic 2HDM

A.L. Cherchiglia,[a,b] **G. De Conto**[c] **and C.C. Nishi**[d]

[a]*Instituto de Física Gleb Wataghin, Universidade Estadual de Campinas,*
Rua Sérgio Buarque de Holanda, 777, 13083-859, Campinas-SP, Brasil

[b]*Departamento de Física Teórica y del Cosmos, Universidad de Granada,*
Campus de Fuentenueva, E-18071 Granada, Spain

[c]*Centro de Ciências Naturais e Humanas, Universidade Federal do ABC,*
Av. dos Estados, 5001, 09.210-170, Santo André-SP, Brasil

[d]*Centro de Matemática, Computação e Cognição, Universidade Federal do ABC,*
Av. dos Estados, 5001, 09.210-170, Santo André-SP, Brasil

E-mail: alche@unicamp.br, george.de.conto@gmail.com,
celso.nishi@ufabc.edu.br

ABSTRACT: One simple way to lower the scale of the seesaw mechanism that generates neutrino masses is to attribute part of their smallness to a suppressed vacuum expectation value of a second Higgs doublet as in the neutrinophilic 2HDM or in the type IB seesaw model. On that structure we add one charged singlet scalar to induce a chirally enhanced contribution to $(g-2)_\mu$ with the same righthanded neutrinos of the seesaw. We discuss the interplay of generating the necessary contribution to the latter with lepton flavor violation which is also necessarily brought to low scale. We show that it is possible to explain $(g-2)_\mu$ even for heavy neutrino masses of order of a few TeV.

Contents

1 Introduction

The observation of neutrino oscillations firmly established that neutrinos have tiny masses and mix in the weak charged current [1]. These properties clearly demonstrate that family lepton numbers associated to the lepton flavors e, μ, τ are not conserved in nature. The origin of both family lepton number violation and of neutrino masses can be naturally attributed to the dimension five Weinberg operator [2] pointing to a natural scale of 10^{12} GeV. If the new physics violating family lepton number appears only at this scale, then its effects, visible primarily on dimension six operators, are expected to be unobservably small. These effects include those of charged lepton flavor violation (CLFV) that are expected to be probed with much greater precision in the coming years.

In contrast, the discrepancy between the experimental and SM prediction for the muon anomalous magnetic moment, $(g-2)_\mu$ or a_μ, is a persistent anomaly that requires TeV scale (or lower) new physics coupling to the muon that may or may not violate lepton flavor. A dedicated program to decrease the experimental uncertainty by a factor of four is

currently ongoing in Fermilab, with the first data analysis released in 2021, and the second in 2023. The value for a_μ combined from the results obtained in Fermilab and Brookhaven is [3, 4] $a_\mu^{\text{Exp}} = (11659205.9 \pm 2.2) \times 10^{-10}$, while the SM prediction from the Muon $g-2$ Theory Initiative White Paper [5–25] is $a_\mu^{\text{SM}} = (11659181.0 \pm 4.3) \times 10^{-10}$, resulting in the 5.1σ discrepancy:

$$\delta a_\mu^{\text{BSM}} = (24.9 \pm 4.8) \times 10^{-10}. \tag{1.1}$$

The SM prediction makes use of dispersion methods to calculate the hadronic contributions that are the major source of uncertainty.[1]

By disregarding neutrino mass generation and minimally introducing new physics that couples to the muon in a flavor conserving fashion or obeying minimal flavor violation, one can explain a_μ [35–38] and still easily avoid large CLFV effects. A critical review of the minimal extensions with one or two new fields can be seen in ref. [39]; see also ref. [40]. If the dominant new physics contribution occurs at 1-loop, a key ingredient is the presence of a *chiral enhancement* that occurs by replacing one chiral flipping coupling involving the muon Yukawa $y_\mu \sim 0.0006$ by an order one coupling [35, 37, 38, 41, 42].

With new physics at the TeV scale, the dipole operator responsible for a_μ should be given by the dimension 6 operator $\bar{\ell}_\mu \sigma^{\alpha\beta} H \mu_R F_{\alpha\beta}$ in the electroweak symmetric phase where the necessary chirality flip $\mu_R \to \mu_L$ involves a Higgs insertion. Then the one-loop contribution to a_μ can be separated into two classes [38, 41] depending on the location of the Higgs insertion: (i) if it occurs in the external muon legs; (ii) if it occurs in one of the internal lines. For contributions of type (i), there is no chiral enhancement because the Higgs insertion is accompanied by the usual muon Yukawa y_μ which also supplies a chiral flipping.[2] If all new fields are electroweak singlets, this is the only possibility. In contrast, chiral enhancement is possible for contributions of type (ii) because the Higgs is attached to a vertex other than the muon Yukawa. Enhancement occurs if this vertex is replaced by the top Yukawa coupling (e.g., with the mediation of leptoquarks [47–49]) or the tau Yukawa coupling (e.g., with lepton flavor changing coupling with an additional Higgs doublet [88]). The large coupling may also come from non-SM interactions such as with vectorlike leptons [37, 50, 51]. In all these examples, the new Higgs insertion also provides a chiral flipping.

With the presence of new scalars mixing with the SM Higgs, enhancement is also possible through the couplings of these new scalars with the muon. In the Two-Higgs-doublet model (2HDM), this feature is available for the types II/X or aligned version with contributions enhanced by $\tan\beta$ (or, similarly, ζ_l for the aligned version). However, in order to accommodate a_μ, some of the scalars must be at the weak scale, which renders

---

[1]There is currently no consensus between the dispersion method and lattice results reported by the BMW collaboration [26]. On the one hand, if the latter is used, the a_μ discrepancy is reduced to 1.5σ level. On the other hand, it disagrees with the R-ratio based prediction used in [5] by more than 2.1σ. Comparison between different lattice groups is under way, with consistent results among them [27–33]. Nevertheless, most of these results stand for specific euclidean windows, not the full determination of hadronic contributions to a_μ. So an investigation of the source of incompatibility among the two approaches is urgent, together with more high precision lattice results. See [34] for an recent evaluation of the different euclidean windows using the dispersion method. In this work, we will adopt the result in eq. (1.1).

[2]It is possible to explain a_μ with a type (i) contribution but either the new states in the loop need to lie at the electroweak scale or lower; see e.g. [43–45] or the couplings are at the edge of perturbativity; see e.g. [46].

only type X [52] or the aligned version [53–56] as possible candidates. For the muon specific 2HDM [57], it is possible to push the scalars to higher masses. In the MSSM, a similar reasoning apply, where the main contributions are also enhanced by $\tan\beta$, allowing to accommodate a_μ (see e.g. [58] for a review). However, differently from the 2HDM versions mentioned, in the MSSM there are innumerous sources of flavor violation that need to be properly suppressed [59, 60]; see e.g. [39] for an updated analysis.

In this work, we aim to connect the physics responsible for a_μ with neutrino masses generation so that the same mediators participate in both processes. We focus on TeV scale mediators and we also seek minimality in their number. Two general features immediately follow. Firstly, the seesaw scale has to be lowered to the TeV scale or lower and, secondly, one certainly cannot impose family lepton number to be conserved so that the interplay with CLFV is crucial. Simply lowering the mediator masses for the type I [61–63], type II [64–68] or type III [69–72] seesaw models do not work because their contribution to a_μ is negative [36, 73].[3] In particular, adding any number of singlet RHNs to implement the type I seesaw mechanism leads to a negative contribution to a_μ [74] even in low-scale seesaw scenarios such as the inverse seesaw [75–77] or the symmetry protected case [78]. This situation does not change if the heavy particles do not participate in the generation of neutrino masses.

Focusing on the seesaw, there are many ways that the seesaw scale can be lowered. The aforementioned inverse seesaw is the case with extended tree level mediators that brings additional suppression due to approximate lepton number conservation. Another option is to consider radiative generation; see ref. [79] for a review and refs. [80–89] for models connecting a_μ with radiative neutrino mass generation. Yet another way is to attribute part of the smallness of neutrino masses to a vacuum expectation value (VEV) of a second Higgs doublet that only couples to neutrinos. This is the neutrinophilic 2HDM (ν-2HDM) for which the RHNs can be Majorana [90, 91] or Dirac [92–96]. Our focus will be on the former as the Majorana mass will induce the chirality flip enhancing the a_μ contribution. An earlier attempt to connect neutrino masses with a_μ considered this neutrinophilic 2HDM with Majorana RHNs [91], where the interplay with CLFV was studied. However, in its simplest form, the new contribution to $(g-2)_\mu$ were negative. Phenomenological studies unrelated to a_μ were performed in refs. [97–99]. A second Higgs doublet with small vev also helps explaining the small neutrino mass in the recently proposed type IB seesaw [100, 101] where two Higgs doublets couple to the two RHNs that form a pseudo-Dirac pair of an approximate U(1) symmetry. Other recent works connecting a_μ with neutrino mass generation can be seen in refs. [46, 102–106].

Here we show that the shortcomings of the ν-2HDM (and also the type IB seesaw) to solve a_μ can be overcome by introducing another field — a charged scalar singlet — to the model so that a chirally enhanced contribution can be generated. This contribution has no definite sign and allows the new fields to be at the TeV scale. Both the Majorana RHNs and the charged scalar contributes to a_μ while the RHNs and the neutrinophilic Higgs doublets are responsible for neutrino masses. In particular, the RHN Majorana mass in

---

[3]Ref. [91] had considered the type II seesaw and its interplay with a_μ but they did not consider the correct sign of the contribution.
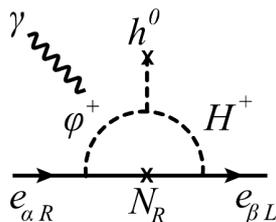
Figure 1. Chirally enhanced contribution to muon $g-2$ involving RHN N_R and charged scalars.

the loop induces the necessarily chirality flip while the Higgs insertion occurs with scalars and it is decoupled from the chiral flipping. Since lepton flavor violation is built in with the TeV scale new physics, it is important to study the induced CLFV processes.

The outline of the paper is as follows. In section 2 we present the models and in section 3 we show how they generate the neutrino masses with TeV scale mediators. Section 4 shows the calculation for a_μ and CLFV observables. Section 5 discusses the interplay between obtaining the correct a_μ and avoiding the constraints of CLFV processes. The summary is given in section 6.

2 Models

We seek scenarios where a_μ is explained with the participation of the righthand neutrinos (RHNs) at one-loop at the same time that these heavy neutrinos generate the necessary active neutrino masses through a low scale seesaw mechanism. More specifically, we require a chiral enhanced contribution to a_μ connecting μ_L with μ_R and then two more charged scalars — one electroweak singlet and another residing in a doublet — are necessary to close the loop as shown in figure 1. From the diagram it is clear that the chiral enhancement will be proportional to the RHN Majorana mass M_N which we require to be at the TeV scale.[4]

So we extend the SM by considering two Higgs doublets Φ_1, Φ_2, two[5] righthanded neutrino (RHN) fields N_{iR}, $i = 1, 2$, and one singlet charged scalar φ^+. The relevant part of the Lagrangian involving the Higgs doublets and the righthanded neutrino fields is

$$-\mathscr{L} \supset \bar{\ell}_\alpha h_\alpha \Phi_e e_{\alpha R} + \bar{N}_{iR} \lambda^{(1)}_{i\alpha} \tilde{\Phi}^\dagger_1 \ell_\alpha + \bar{N}_{iR} \lambda^{(2)}_{i\alpha} \tilde{\Phi}^\dagger_2 \ell_\alpha + \frac{1}{2} \bar{N}_{iR} (M_R)_{ij} N^c_{jR} + h.c., \quad (2.1)$$

where ℓ_α, $\alpha = e, \mu, \tau$ are the lepton doublets and Φ_e is Φ_1 or Φ_2 depending on the model. The relevant interaction terms involving the charged singlet scalar is

$$-\mathscr{L} \supset \mu_\varphi \Phi_2^\mathsf{T} \epsilon \Phi_1 \varphi^- + f_{i\alpha} \bar{N}_{iR} e^c_{\alpha R} \varphi^- + h.c., \quad (2.2)$$

where we choose μ_φ real without loss of generality. The interaction term $\overline{\ell^c_\alpha} \ell_\beta \varphi^+$ is absent owing to the symmetries of the specific models introduced below and then there is no

---

[4]This is one of the minimal possibilities considered in ref. [38] to explain $(g-2)_\mu$ and DM stabilized by an unbroken $\mathbb{Z}_2$ leading to an inert Higgs doublet. Here the additional Higgs doublet has a small vev that helps explaining small neutrino masses.

[5]These two neutrinos will generate the minimal number of two nonzero light neutrino masses but three RHNs can be equally considered.

radiative neutrino mass generation as in the Zee model [107].[6] This absence also forbids the generation of four-fermion operators ℓ^4 from tree level φ^+ exchange.

One of the simplest models within the type I seesaw is to suppress the Dirac mass term by attributing its origin to a Higgs doublet different from the rest, with tiny vacuum expectation value. This is the neutrinophilic 2HDM model (ν-2HDM) [90] which is obtained from (2.1) by imposing a $\mathbb{Z}_2$ where N_{iR}, Φ_1 are odd. As a consequence, $\lambda^{(2)} = 0$ and $\Phi_e = \Phi_2$. The singlet scalar φ^+ is additional and we assume it is odd so that the terms in (2.2) are allowed. The resulting Lagrangian is

$$
\begin{aligned}
-\mathscr{L}_{\nu\text{-2HDM}} \supset{}& \bar{\ell}_\alpha h_\alpha \Phi_2 e_{\alpha R} + \bar{N}_{iR} \lambda^{(1)}_{i\alpha} \tilde{\Phi}^\dagger_1 \ell_\alpha + \frac{1}{2} \bar{N}_{iR} M_{N_i} N^c_{iR} \\
&+ \mu_\varphi \Phi^\mathsf{T}_2 \epsilon \Phi_1 \varphi^- + f_{i\alpha} \bar{N}_{iR} e^c_{\alpha R} \varphi^- + h.c.
\end{aligned}
\tag{2.3}
$$

The doublet $\Phi_2 \approx H_{\text{SM}}$ will be mostly the SM Higgs doublet while $\Phi_1 \approx H_\nu$ will be mostly composed of non-SM higgses. Neutrino masses will depend solely on $\langle \Phi^0_1 \rangle = v_1$ which will be suppressed.

Another minimal possibility is to combine the righthanded neutrinos into a (pseudo)Dirac pair through a $\mathrm{U}(1)_N$ symmetry with charges [100, 101]

$$
N_{1R} \sim \Phi_1 \sim +1\,, \quad N_{2R} \sim \Phi_2 \sim -1\,.
\tag{2.4}
$$

It leads to the Lagrangian

$$
-\mathscr{L}_{\text{Ib}} \supset \bar{N}_{R1} \lambda_{1\alpha} \tilde{\Phi}^\dagger_1 \ell_\alpha + \bar{N}_{R2} \lambda_{2\alpha} \tilde{\Phi}^\dagger_2 \ell_\alpha + M \overline{N^c_{R1}} N_{R2} + h.c.
\tag{2.5}
$$

and the seesaw mechanism is dubbed seesaw type IB. Compared to (2.1), we are already simplifying the notation in that $\lambda^{(1)}_{1\alpha} = \lambda_{1\alpha}$ and $\lambda^{(2)}_{2\alpha} = \lambda_{2\alpha}$ whereas $\lambda^{(1)}_{2\alpha} = \lambda^{(2)}_{1\alpha} = 0$. The other couplings depend on the choice of $\mathrm{U}(1)_N$ charges for $e_{R\alpha}$ and φ. We adopt the charges $e_R \sim -1$ and $\varphi^- \sim -2$ so that

$$
-\mathscr{L}_{\text{Ib}} \supset h_\alpha \bar{\ell}_\alpha \Phi_1 e_{R\alpha} + f_{2\alpha} \bar{N}_{2R} e^c_{\alpha R} \varphi^- + \mu_\varphi \Phi^\mathsf{T}_2 \epsilon \Phi_1 \varphi^- + h.c.
\tag{2.6}
$$

To keep h_τ within perturbative values, we need $v_1 \gtrsim 10^{-2} v$ and most of the suppression for light neutrino masses should still come from the suppression of the Yukawas $\lambda_{j\alpha}$. We could flip the charges of e_R and φ^- and then replace Φ_1 by Φ_2 in the first term and N_{2R} by N_{1R} in the second. But even in this case we cannot suppress v_1 too much because the dominant $g-2$ contribution is proportional to $v_1 \lambda_{2\alpha}$. The third term softly breaks the $\mathrm{U}(1)_N$ symmetry[7] which cannot be exact as a global symmetry to avoid unwanted massless scalars. The model in ref. [100], for example, imposes a $\mathbb{Z}_3$ instead of $\mathrm{U}(1)_N$.

---

[6]A recent paper considered the Zee model for $(g-2)_{e,\mu}$ [88], where the couplings to charged singlet are not relevant and a_μ is explained by the contributions of the additional Higgs doublet with a chiral enhancement at one-loop of at most the τ Yukawa. Ref. [89] considered the complementary case of two charged scalar singlets and one RHN where neutrino masses are radiative but there is no chirally enhanced contribution to a_μ.

[7]The quadratic term $\Phi^\dagger_2 \Phi_1$ should be added as well. The term $\ell\ell\varphi^+$ remains forbidden.

For both models, the charged scalar component that is dominant in the non-SM Higgs doublet behaves as the charged scalar in the type I 2HDM and they are only constrained by LEP [108]:

$$M_{H^+} > 75 \, \text{GeV} \, . \tag{2.7}$$

On the other hand, the singlet component couples solely with charged leptons and righthand neutrino, implying that the model independent constraint from LEP does not apply. Since we allow for a small mixing, we will consider that both charged scalars will have masses around the electroweak scale or above.

3 Light neutrino masses

Light neutrino masses are generated from the type I seesaw, i.e., through the exchange of RHNs in (2.1) at tree level. The generated effective Weinberg operator is

$$\mathscr{L} = \frac{1}{2} \bar{\ell}_\alpha^c \Gamma_{\alpha i}^\mathsf{T} (M_R^{-1})_{ij} \Gamma_{j\beta} \ell_\beta + h.c. \, , \tag{3.1}$$

depending on the two Higgs doublets through

$$\Gamma_{j\beta} = \lambda_{j\beta}^{(1)} \tilde{\Phi}_1^\dagger + \lambda_{j\beta}^{(2)} \tilde{\Phi}_2^\dagger \, . \tag{3.2}$$

3.1 ν-2HDM model

For the ν-2HDM model, only Φ_1 participates in the seesaw and $\lambda^{(2)} = 0$. Then the neutrino mass matrix is given by

$$M_\nu = -v_1^2 \lambda^{(1)\mathsf{T}} M_R^{-1} \lambda^{(1)} \, , \tag{3.3}$$

where its lightness is partly explained by $\langle \Phi_1^0 \rangle = v_1 \ll v = \sqrt{v_1^2 + v_2^2} = 174 \, \text{GeV}$. If $M_R \sim \text{TeV}$, we need

$$v_1 \lambda^{(1)}/v \sim \frac{\sqrt{M_R M_\nu}}{v} \lesssim \frac{\sqrt{1 \, \text{TeV} \times 0.05 \, \text{eV}}}{v} \sim 10^{-6} \, . \tag{3.4}$$

We can choose $v_1/v \sim 10^{-6}$ in order to have $\lambda^{(1)}$ of order one to address the deviation in a_μ.

Since we are focusing on the minimal case of two RHNs, the heavy neutrino Yukawa coupling $\lambda^{(1)}$ is mostly fixed by the masses and mixing of light neutrinos. Using the Casas-Ibarra parametrization, we can write for normal ordering (NO),

$$\begin{aligned} v_1 \lambda_{1\alpha}^{(1)} &= i\sqrt{M_1} \big(\sqrt{m_2} c_z V_{2\alpha}^\dagger - \sqrt{m_3} s_z V_{3\alpha}^\dagger \big) \, , \\ v_1 \lambda_{2\alpha}^{(1)} &= i\sqrt{M_2} \big(\sqrt{m_2} s_z V_{2\alpha}^\dagger + \sqrt{m_3} c_z V_{3\alpha}^\dagger \big) \, , \end{aligned} \tag{3.5}$$

where $c_z = \cos z$ and $s_z = \sin z$ depend on the free complex angle z. We are taking $M_R = \text{diag}(M_1, M_2)$ and the neutrino mass matrix in (3.3) is $M_\nu = V^* \text{diag}(0, m_2, m_3) V^\dagger$, with V being the PMNS matrix. Therefore, besides the two CP phases in V, we have five free parameters in the neutrino sector: $M_1, M_2, \text{Re}(z), \text{Im}(z), \tan\beta = v_2/v_1$. Note that for $M_1 = M_2$, the real part of z is not physical.

For inverted ordering (IO), we have instead

$$v_1\lambda_{1\alpha}^{(1)} = i\sqrt{M_1}\big(\sqrt{m_1}c_z V_{1\alpha}^\dagger - \sqrt{m_2}s_z V_{2\alpha}^\dagger\big)\,,$$
$$v_1\lambda_{2\alpha}^{(1)} = i\sqrt{M_2}\big(\sqrt{m_1}s_z V_{1\alpha}^\dagger + \sqrt{m_2}c_z V_{2\alpha}^\dagger\big)\,. \tag{3.6}$$

The only difference in this case is that $M_\nu = V^* \mathrm{diag}(m_1, m_2, 0)V^\dagger$.

3.2 Type Ib seesaw model

For the type IB seesaw model, the neutrino mass matrix coming from (3.1) is

$$(M_\nu)_{\alpha\beta} = -\frac{v_1 v_2}{M}(\lambda_{1\alpha}\lambda_{2\beta} + \lambda_{2\alpha}\lambda_{1\beta})\,, \tag{3.7}$$

where $v_a = \langle\Phi_a^0\rangle$, $a = 1, 2$, and the Yukawa couplings are defined in (2.5). We choose $v_1 < v_2$ because Φ_2 is the doublet coupling to the charged leptons in (2.6). Adapting (3.4) to this case with $M \sim \mathrm{TeV}$, we obtain

$$\frac{1}{v}\sqrt{v_1\lambda_{1\alpha}v_2\lambda_{2\beta}} \sim \frac{\sqrt{M_R M_\nu}}{v} \lesssim \frac{\sqrt{1\,\mathrm{TeV}\times 0.05\,\mathrm{eV}}}{v} \sim 10^{-6}\,. \tag{3.8}$$

As in the ν-2HDM model, the Yukawa couplings $\lambda_{1\alpha}$ and $\lambda_{2\alpha}$ are mostly fixed by light neutrino masses and mixing.

For NO, the Yukawa couplings can be parametrized as

$$\lambda_{1\alpha} = i\kappa\left(\frac{M}{2v_1 v_2}\right)^{1/2}\left[+i\sqrt{m_2}\,V_{2\alpha}^\dagger + \sqrt{m_3}\,V_{3\alpha}^\dagger\right]\,,$$
$$\lambda_{2\alpha} = i\kappa^{-1}\left(\frac{M}{2v_1 v_2}\right)^{1/2}\left[-i\sqrt{m_2}\,V_{2\alpha}^\dagger + \sqrt{m_3}\,V_{3\alpha}^\dagger\right]\,, \tag{3.9}$$

where we use a different but equivalent parametrization with respect to refs. [100, 101]. Flipping the sign in front of $\sqrt{m_2}$ is equivalent and this sign can be absorbed by flipping the sign of ν_{2L}. The parameter κ is free and can be chosen real by rephasing N_{1R}, N_{2R} with opposite phases. For IO, we can analogously parametrize

$$\lambda_{1\alpha} = i\kappa\left(\frac{M}{2v_1 v_2}\right)^{1/2}\left[+i\sqrt{m_1}\,V_{1\alpha}^\dagger + \sqrt{m_2}\,V_{2\alpha}^\dagger\right]\,,$$
$$\lambda_{2\alpha} = i\kappa^{-1}\left(\frac{M}{2v_1 v_2}\right)^{1/2}\left[-i\sqrt{m_1}\,V_{1\alpha}^\dagger + \sqrt{m_2}\,V_{2\alpha}^\dagger\right]\,. \tag{3.10}$$

Note that in the neutrino sector, besides the unknown CP phases, there are only three free parameters: $M, \tan\beta, \kappa$. This is the same number as the neutrinophilic case with equal masses for the RHNs.

4 Dipole moments and CLFV

Using an effective theory approach, the operators relevant to lepton dipole moments and charged lepton flavor violation (CLFV) processes are the photonic operators

$$\begin{aligned}\mathscr{L}_{\gamma\text{-eff}} = &-\Big(C_{\alpha\beta}^{\sigma R}\bar{e}_{\alpha L}\sigma_{\mu\nu}e_{\beta R}F^{\mu\nu} + h.c.\Big)\\ &-\Big(C_{\alpha\beta}^{\text{ND-}L}\bar{e}_{\alpha L}\gamma_\nu e_{\beta L} + C_{\alpha\beta}^{\text{ND-}R}\bar{e}_{\alpha R}\gamma_\nu e_{\beta R}\Big)\partial_\mu F^{\mu\nu}\,.\end{aligned} \tag{4.1}$$
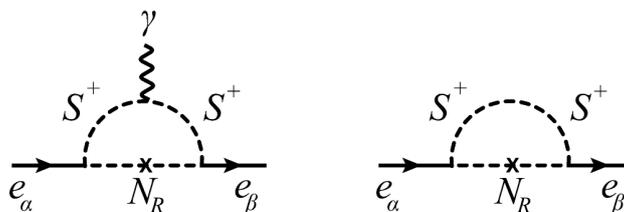
Figure 2. Dipole and self-energy contribution to flavor changing processes.

The operator in the first line is the dipole contribution whereas the ones in the second line are the non-dipole (ND) part. We can see that only the dipole part involves chirarity flipping and chiral enhancement will be possible only for this term. The Wilson coefficients at 1-loop can be obtained by matching the full theory with the effective theory through appropriate 1-loop amplitudes. The relevant amplitudes come from the dipole (left) and self-energy (right) diagrams in figure 2.

4.1 Dipole moments and $\ell_\alpha \to \ell_\beta \gamma$

The Wilson coefficient of the dipole operator contributes to the dipole moments and $\ell_\alpha \to \ell_\beta \gamma$ as

$$
a_\alpha = -\frac{4m_\alpha}{e} \operatorname{Re}(C_{\alpha\alpha}^{\sigma R}),
$$
$$
d_\alpha = -2 \operatorname{Im}(C_{\alpha\alpha}^{\sigma R}),
$$
$$
\operatorname{Br}[\ell_\alpha \to \ell_\beta \gamma] = \frac{m_\alpha^3}{4\pi\Gamma_\alpha}(|C_{\alpha\beta}^{\sigma R}|^2 + |C_{\beta\alpha}^{\sigma R}|^2),
$$

(4.2)

where a_α, d_α are the contributions to the magnetic and eletric dipole moments, respectively. These formulas assume that our covariant derivative in QED is $D_\mu = \partial_\mu + ieQA_\mu$ and similarly for the SM.

For the ν-2HDM described in (2.3), $\Phi_2 \approx H_{\mathrm{SM}}$ and $\Phi_1 \approx H_\nu$ is almost inert with a tiny vev. The chirally enhanced contribution to the dipole operator is given in figure 1, with φ being the charged singlet, H^+ being essentially the charged Higgs residing in Φ_1 and h^0 being the SM Higgs boson. The chiral enhancement comes from the N_{iR} Majorana masses, M_{N_i}, and these heavy neutrinos only couple to Φ_1. The expected chirally enhanced contribution is then of the form

$$
C_{\beta\alpha}^{\sigma R} \sim \frac{ev_2\mu_\varphi}{(4\pi)^2\Lambda^4} \lambda_{\beta i}^{(1)\dagger} M_{N_i} f_{i\alpha}^*,
$$

(4.3)

where the transferred momentum is $q^2 = -m_\mu^2$.

For the exact contribution we need to include the mixing between the charged higgs H^+ in the doublet and the scalar singlet φ^+ coming from the μ_φ term in (2.3) or (2.2). The contribution in the scalar potential is

$$
\mu_\varphi\varphi^-(\Phi_2^+\Phi_1^0 - \Phi_2^0\Phi_1^+) \to -\mu_\varphi v \varphi^- H^+,
$$

(4.4)

where $vH^+ \equiv v_2\Phi_1^+ - v_1\Phi_2^+$, $v_i = \langle\Phi_i^0\rangle$, is the physical charged Higgs field within the doublets when $\mu_\varphi = 0$. The orthogonal direction is the charged Goldstone absorbed by

the W. Considering arbitrary mass terms for $H^+ H^-$ and $\varphi^+ \varphi^-$, the mixing term (4.4) induces the mixing

$$\begin{pmatrix} H^+ \\ \varphi^+ \end{pmatrix} = \begin{pmatrix} c_\gamma & -s_\gamma \\ s_\gamma & c_\gamma \end{pmatrix} \begin{pmatrix} S_1^+ \\ S_2^+ \end{pmatrix} , \tag{4.5}$$

with angle

$$\sin 2\gamma = -\frac{2\mu_\varphi v}{M_{S_2}^2 - M_{S_1}^2} , \tag{4.6}$$

and S_i^+ are the charged scalars with masses M_{S_i}, $i = 1, 2$. We have chosen $M_{S_2} > M_{S_1}$.

Then the complete contribution arising from the diagrams in figure 2 is

$$\frac{16\pi^2}{e} C_{\beta\alpha}^{\sigma R} = c_\gamma s_\gamma \frac{v_2}{v} \sum_j \frac{\lambda_{\beta j}^{(1)\dagger} f_{j\alpha}^*}{M_{N_j}} \left[x_{2j} f_S(x_{2j}) - x_{1j} f_S(x_{1j}) \right] , \tag{4.7a}$$

$$+ \ m_\alpha \frac{v_2^2}{v^2} \sum_j \lambda_{\beta j}^{(1)\dagger} \left[\frac{c_\gamma^2}{M_{S_1}^2} \tilde{f}_S(x_{1j}) + \frac{s_\gamma^2}{M_{S_2}^2} \tilde{f}_S(x_{2j}) \right] \lambda_{j\alpha}^{(1)} \tag{4.7b}$$

$$+ m_\beta \sum_j f_{\beta j}^{\mathsf{T}} \left[\frac{s_\gamma^2}{M_{S_1}^2} \tilde{f}_S(x_{1j}) + \frac{c_\gamma^2}{M_{S_2}^2} \tilde{f}_S(x_{2j}) \right] f_{j\alpha}^* , \tag{4.7c}$$

where $x_{kj} \equiv M_{N_j}^2 / M_{S_k}^2$ and the loop functions are [37, 38]

$$\begin{aligned} f_S(x) &\equiv \frac{x^2 - 1 - 2x \log x}{4(x-1)^3} , \\ \tilde{f}_S(x) &\equiv \frac{2x^3 + 3x^2 - 6x + 1 - 6x^2 \log x}{24(x-1)^4} . \end{aligned} \tag{4.8}$$

See appendix A for the details. We have checked that the contribution proportional to $(\lambda^{(1)})^2$ matches ref. [99] for $\gamma = 0$.

Let us discuss the various contributions. The first contribution (4.7a) is the chirally enhanced (left-right), reducing to (4.3) when $M_{S_i} \gg M_{N_j}$ as $f_S(0) = 1/4$ and we identify $\Lambda^4 = 4M_{S_2}^2 M_{S_1}^2 (M_{S_2}^2 - M_{S_1}^2)$. The contributions (4.7b) and (4.7c) are not chirally enhanced (left-left and right-right respectively) as the chiral flip comes from the external lines. So the chirally enhanced contribution is larger than the non-chirally enhanced contributions by a factor

$$c_\gamma s_\gamma \frac{M_S^2}{m_\mu M_N} \sim c_\gamma s_\gamma \times 10^4 , \tag{4.9}$$

for order one couplings and the numbers assume $M_N \sim M_{S_i} \sim \text{TeV}$. Given the definition of the angle γ in (4.6) the trilinear coupling μ_φ cannot be arbitrarily small if we require the chirally enhanced contribution to dominate:

$$|\mu_\varphi| \gtrsim 1 \, \text{GeV} \quad \text{or} \quad |s_\gamma| \gtrsim 10^{-4} . \tag{4.10}$$

The dominance of the chirally enhanced contribution is important because the non-chirally enhanced contributions are positive definite and leads to a contribution to a_μ which is negative definite, contrary to the experimental observation. They are similar to the contribution of N_R exchange in the usual seesaw models [36, 74].

Observable	Current limit	Future limit
$\mathrm{Br}(\mu \to eee)$	$< 1.0 \times 10^{-12}$[109]	10^{-16}[110]
$\mathrm{Br}(\tau \to \mu\mu\mu)$	$< 2.1 \times 10^{-8}$[111]	3.4×10^{-10}[112]
$\mathrm{Br}(\tau \to \mu ee)$	$< 8.4 \times 10^{-9}$[111]	2.9×10^{-10}[112]
$\mathrm{Br}(\tau \to eee)$	$< 1.4 \times 10^{-8}$[111]	4.3×10^{-10}[112]
$\mathrm{Br}(\tau \to e\mu\mu)$	$< 1.6 \times 10^{-8}$[111]	4.3×10^{-10}[112]
$\mathrm{Br}(\mu \to e\gamma)$	$< 4.2 \times 10^{-13}$[109]	6×10^{-14}[113]
$\mathrm{Br}(\tau \to \mu\gamma)$	$< 4.4 \times 10^{-8}$[109]	10^{-9}[112]
$\mathrm{Br}(\tau \to e\gamma)$	$< 3.3 \times 10^{-8}$[109]	3×10^{-9}[112]
$\Gamma^{\mathrm{conv}}_{\mu \to e}/\Gamma^{\mathrm{capt}}_N$	$< 7.0 \times 10^{-13}$[114]*	3×10^{-17}[115–119]**/10^{-18}[120]†

Table 1. Current and future limits for charged lepton flavor violating processes at 90% CL. For μe conversion, the nucleous is Au (*) and Al (**) or Ti (†).

For the type IB model in (2.5) and (2.6), the estimate of the chirally enhanced contribution analogous to (4.3) will be

$$C^{\sigma R}_{\beta\alpha} \sim \frac{v_2 \mu_\varphi}{(4\pi)^2 \Lambda^4} \lambda^\dagger_{\beta 1} M f^*_{2\alpha}. \tag{4.11}$$

Then we need $\lambda_{1\beta}$ to be of order one while $\lambda_{2\beta}$ needs to be suppressed due to neutrino masses, cf. (3.8).

The complete contribution reads

$$\frac{16\pi^2}{e} C^{\sigma R}_{\beta\alpha} = c_\gamma s_\gamma \frac{v_2}{v} \frac{\lambda^\dagger_{\beta 1} f^*_{2\alpha}}{M_N} \left[x_2 f_S(x_2) - x_1 f_S(x_1)\right], \tag{4.12a}$$

$$+ \ m_\alpha \frac{v_2^2}{v^2} \lambda^\dagger_{\beta 1} \left[\frac{c_\gamma^2}{M_{S_1}^2} \tilde{f}_S(x_1) + \frac{s_\gamma^2}{M_{S_2}^2} \tilde{f}_S(x_2)\right] \lambda_{1\alpha} \tag{4.12b}$$

$$+ m_\beta f^{\mathsf{T}}_{\beta 2} \left[\frac{s_\gamma^2}{M_{S_1}^2} \tilde{f}_S(x_1) + \frac{c_\gamma^2}{M_{S_2}^2} \tilde{f}_S(x_2)\right] f^*_{2\alpha}, \tag{4.12c}$$

where $x_i = M_N^2/M_{S_i^2}$. We have neglected additional contributions proportional to $\lambda^*_{2\beta} \lambda_{2\alpha} v_1^2$ which will be highly suppressed. Here the requirement (4.10) is equally necessary for order one couplings.

In table 1 we show the current and future limits for different $\ell_\alpha \to \ell_\beta \gamma$. Limits for other CLFV processes are also shown.

4.2 μ-e conversion in nuclei

A very stringent test for CFLV is the coherent μ^--e^- conversion in a muonic atom of nucleus (A, Z) by neutrinoless muon capture

$$\mu^- + (A, Z) \to e^- + (A, Z),$$

mediated in our case by the effective flavor-changing photon interactions in (4.1). We neglect similar Z mediated processes which are suppressed by the Z mass. It should be noticed that, contrary to $\mu \to e\gamma$ decay, one needs to consider off-shell photon emission. The general photonic $\mu-e$ transition amplitude is given by [121]

$$\mathcal{M} = -eA_\mu^*(q)\bar{u}_e(p_e)\left[(f_{E0} + \gamma_5 f_{M0})\gamma_\nu\left(g^{\mu\nu} - \frac{q^\mu q^\nu}{q^2}\right) + (f_{M1} + \gamma_5 f_{E1})\frac{i\sigma_{\mu\nu}q^\nu}{m_\mu}\right]u_\mu(p_\mu),$$
(4.13)

where p_μ and p_e are the momenta of the muon and electron respectively, $q = p_\mu - p_e$ is the transfered momentum, and $f_X \equiv f_X(q^2)$ are form factors. In the case of $\mu \to e\gamma$ decay, only the dipole part (f_{E1}, f_{M1}) contributes. The form factors can be written in terms of the Wilson coefficients introduced in (4.1):

$$f_{E0} = (C_{e\mu}^{\text{ND-}L} + C_{e\mu}^{\text{ND-}R})\frac{q^2}{2e}, \qquad f_{M0} = (C_{e\mu}^{\text{ND-}L} - C_{e\mu}^{\text{ND-}R})\frac{q^2}{2e}, \qquad (4.14)$$

$$f_{E1} = -(C_{e\mu}^{\sigma R} - C_{\mu e}^{\sigma R*})\frac{m_\mu}{e}, \qquad f_{M1} = -(C_{e\mu}^{\sigma R} + C_{\mu e}^{\sigma R*})\frac{m_\mu}{e}. \qquad (4.15)$$

In the approximation pioneered by Weinberg and Feinberg [122], only the photonic contribution is included in the calculation of the branching ratio of the coherent $\mu - e$ conversion which is given by

$$\text{Br}[\mu N \to eN] \equiv \frac{\Gamma[\mu N \to eN]}{\Gamma_{\text{capt}}} = \frac{8m_\mu\alpha^5 Z_{\text{eff}}^4 Z|F_p|^2\xi^2}{\Gamma_{\text{capt}}}. \qquad (4.16)$$

Here Z_{eff} is an effective atomic charge due to averaging the muon wave function over the nuclear density, Γ_{capt} is the total muon capture rate, and ξ^2 is obtained with knowledge of the form factors

$$\xi^2 = |f_{E0}(-m_\mu^2) + f_{M1}(-m_\mu^2)|^2 + |f_{E1}(-m_\mu^2) + f_{M0}(-m_\mu^2)|^2, \qquad (4.17)$$

where we use the transferred momentum $q^2 = -m_\mu^2$.

In general, the non-photonic part should be included as well, which is parametrized by an effective four-fermion interaction containing quarks. In our particular case, these contributions would come from box diagrams containing both the righthanded neutrinos and charged scalars. Since the coupling between quarks and the charged scalars is suppressed (it will be proportional to the ratio v_1/v_2), we can safely neglect these diagrams.

Finally, we rewrite the branching ratio in terms of the Wilson coefficients, to allow a straightforward application to our model

$$\text{Br}[\mu N \to eN] = \frac{4m_\mu^3\alpha^4 Z_{\text{eff}}^4 Z|F_p|^2}{\pi\Gamma_{\text{capt}}}\left(\left|C_{e\mu}^{\sigma R} + \frac{m_\mu}{2}C_{e\mu}^{\text{ND-L}}\right|^2 + \left|C_{\mu e}^{\sigma R} + \frac{m_\mu}{2}(C_{e\mu}^{\text{ND-R}})^*\right|^2\right). \qquad (4.18)$$

In our case, for order one couplings and loop functions, the chiral enhanced part in the dipole contribution will dominate the non-dipole part by a factor $M_{S_i}/m_\mu \sim M_{N_k}/m_\mu \sim 10^4$ for the new fields in the TeV scale and s_γ not too small as (4.10). In this case of dipole dominance, the ratio $\text{Br}[\mu N \to eN]/\text{Br}(\mu \to e\gamma)$ depends roughly only on the atomic

$_Z^A$Nucleus	Z_{eff}	F_p	Γ_{capt}(GeV)
$_{13}^{27}$Al	11.5	0.64	4.64×10^{-19}
$_{22}^{48}$Ti	17.6	0.54	1.70×10^{-18}
$_{38}^{80}$Sr	25.0	0.39	4.62×10^{-18}
$_{51}^{121}$Sb	29.0	0.32	6.72×10^{-18}
$_{79}^{197}$Au	33.5	0.16	8.60×10^{-18}
$_{82}^{207}$Pb	34.0	0.15	8.85×10^{-18}

Table 2. Values for Z_{eff}, F_p, and Γ_{capt}(GeV) for different nuclei [125, 126].

number of the nucleous [123] and we have checked it for our case. As for the non-dipole part, we have found that the relative sign between $C^{\sigma R}$ and C^{ND} in (4.18) is effectively opposite to refs. [99, 124, 125].

At present, the best limit for this branching ratio comes from conversion in gold nuclei [114]: $\Gamma_{\text{conv}}^{\text{Au}}/\Gamma_{\text{capt}}^{\text{Au}} < 7.0 \times 10^{-13}$, where $\Gamma_{\text{capt}}^{\text{Au}} = 8.7 \times 10^{-18}$ GeV. There are, however, future experiments that aim to reduce the bounds on $\mu - e$ conversion by several orders of magnitude [115–119]. Their aim is to achieve $\Gamma_{\text{conv}}^{\text{Al}}/\Gamma_{\text{capt}}^{\text{Al}} < 3 \times 10^{-17}$ using aluminium nuclei. The different effective parameters for different nucleous are shown in table 2.

The Wilson coefficient of the non-dipole part can be obtained for the ν-2HDM model as

$$
\begin{aligned}
\frac{16\pi^2}{e} C_{\beta\alpha}^{\text{ND-}L} &= \frac{v_2^2}{v^2} \sum_j \lambda_{\beta j}^{(1)\dagger} \lambda_{j\alpha}^{(1)} \left[c_\gamma^2 \frac{G_S(x_{1j})}{6M_{S_1}^2} + s_\gamma^2 \frac{G_S(x_{2j})}{6M_{S_2}^2} \right], \\
\frac{16\pi^2}{e} C_{\beta\alpha}^{\text{ND-}R} &= \sum_j f_{\beta j}^{\mathsf{T}} f_{j\alpha}^* \left[s_\gamma^2 \frac{G_S(x_{1j})}{6M_{S_1}^2} + c_\gamma^2 \frac{G_S(x_{2j})}{6M_{S_2}^2} \right],
\end{aligned}
\tag{4.19}
$$

where the loop function is

$$
G_S(x) = \frac{2 - 9x + 18x^2 - 11x^3 + 6x^3 \log(x)}{6(1-x)^4}.
\tag{4.20}
$$

The latter function is the same as $G_2(x)$ in ref. [99]. See details in appendix A. As anticipated, there is no chiral enhancement for these coefficients.

For the type IB seesaw model, we analogously obtain

$$
\begin{aligned}
\frac{16\pi^2}{e} C_{\beta\alpha}^{\text{ND-}L} &= \frac{v_2^2}{v^2} \lambda_{\beta 1}^{\dagger} \lambda_{1\alpha} \left[c_\gamma^2 \frac{G_S(x_1)}{6M_{S_1}^2} + s_\gamma^2 \frac{G_S(x_2)}{6M_{S_2}^2} \right], \\
\frac{16\pi^2}{e} C_{\beta\alpha}^{\text{ND-}R} &= f_{\beta 2}^{\mathsf{T}} f_{2\alpha}^* \left[s_\gamma^2 \frac{G_S(x_{1j})}{6M_{S_1}^2} + c_\gamma^2 \frac{G_S(x_{2j})}{6M_{S_2}^2} \right].
\end{aligned}
\tag{4.21}
$$

We could also consider the decay $\mu \to eee$. In addition to the Wilson coefficients that we already have, we will need to consider box diagrams. These diagrams have righthanded neutrinos and charged scalars inside, whose contributions will be of the form

$$
f_{i\mu} f_{ie} f_{je} f_{je}, \quad \lambda_{i\mu} \lambda_{ie} \lambda_{je} \lambda_{je}, \quad \lambda_{i\mu} f_{ie} \lambda_{je} f_{je}, \quad f_{i\mu} \lambda_{ie} f_{je} \lambda_{je}
$$

In section 5 we will see that we need suppressed f_{ie} to evade CLFV constraints and still be able to account for $(g-2)_\mu$. In this case, only the contribution with λ survives which is subdominant [99].

5 Solving $(g-2)_\mu$ avoiding CLFV

By considering only the dominant chirally enhanced contribution to the dipole term, we can estimate the interplay between the necessary contribution to a_μ and the necessary suppression to avoid significant CLFV processes. The contribution to a_μ in (4.2) necessary to explain the experimental deviation (1.1) requires

$$|C_{\mu\mu}^{\sigma R}| \sim |\operatorname{Re} C_{\mu\mu}^{\sigma R}| \sim 2 \times 10^{-9}\,\mathrm{GeV}^{-1}\,. \tag{5.1}$$

On the other hand, the current limit on $\mu \to e\gamma$ requires

$$\sqrt{|C_{\mu e}^{\sigma R}|^2 + |C_{e\mu}^{\sigma R}|^2} < 4 \times 10^{-14}\,\mathrm{GeV}^{-1}\,. \tag{5.2}$$

So it is necessary that

$$\frac{\sqrt{|C_{\mu e}^{\sigma R}|^2 + |C_{e\mu}^{\sigma R}|^2}}{|C_{\mu\mu}^{\sigma R}|} \lesssim 2 \times 10^{-5}\,. \tag{5.3}$$

The expected future limit will decrease this number by a factor 2.6. A similar analysis on the current limit on μe conversion in gold nuclei requires

$$\sqrt{|C_{\mu e}^{\sigma R}|^2 + |C_{e\mu}^{\sigma R}|^2} < 10^{-12}\,\mathrm{GeV}^{-1}\,, \tag{5.4}$$

which implies

$$\frac{\sqrt{|C_{\mu e}^{\sigma R}|^2 + |C_{e\mu}^{\sigma R}|^2}}{|C_{\mu\mu}^{\sigma R}|} \lesssim 5 \times 10^{-4}\,. \tag{5.5}$$

The expected future limit in aluminium nuclei will greatly reduce the limit in (5.4) to $6 \times 10^{-15}\,\mathrm{GeV}^{-1}$ and then the bound in (5.5) becomes 3×10^{-6}.

Now, let us see how our models can satisfy the hierarchy (5.3) between flavor changing and flavor conserving couplings to the muon.

We start with the type IB seesaw model. We assume the dominance of the chirally enhanced contribution and require $|s_\gamma| \gg 10^{-4}$ due to (4.10). In this model, to have appreciable a_μ, we need

$$\lambda_{1\mu}^* f_{2\mu}^* \sim O(1)\,. \tag{5.6}$$

On the other hand, according to (5.3), we need $|\lambda_{1\mu}^* f_{2e}^*|, |\lambda_{1e}^* f_{2\mu}^*|$ to be less than 10^{-5}. Since $\lambda_{1\mu}$ needs to be order one, we can adopt $f_{2e} = 0$ for simplicity. In this case,

$$\frac{\sqrt{|C_{\mu e}^{\sigma R}|^2 + |C_{e\mu}^{\sigma R}|^2}}{|C_{\mu\mu}^{\sigma R}|^2} \approx \frac{|\lambda_{1e}|}{|\lambda_{1\mu}|} \gtrsim 0.1\,, \tag{5.7}$$

from the dependence of $\lambda_{1\alpha}$ on neutrino masses and mixing for NO or IO, cf. eqs. (3.9) or (3.10), and (5.3) is never satisfied. Turning on the coupling f_{2e} only worsens the situation

and the type IB seesaw model augmented with a singly charged singlet cannot account for $(g-2)_\mu$ without violating current bounds on $\mu \to e\gamma$.

We now turn to the ν-2HDM model. For appreciable a_μ, assuming the dominance of chirally enhanced contribution, we need large $\mu\mu$ couplings:

$$\lambda_{\mu 1}^{(1)\dagger} f_{1\mu}^*, \ \lambda_{\mu 2}^{(1)\dagger} f_{2\mu}^* \sim O(1)\,. \tag{5.8}$$

For equal masses $M_1 = M_2$, to suppress CLFV processes, we need suppressed μe couplings:

$$|\lambda_{\mu 1}^{(1)\dagger} f_{1e}^* + \lambda_{\mu 2}^{(1)\dagger} f_{2e}^*| \lesssim 10^{-5}\,, \quad |\lambda_{e1}^{(1)\dagger} f_{1\mu}^* + \lambda_{e2}^{(1)\dagger} f_{2\mu}^*| \lesssim 10^{-5}\,. \tag{5.9}$$

Considering (5.8), the first combination vanishes if

$$f_{1e} = f_{2e} = 0\,, \tag{5.10}$$

while the vanishing of the second requires the orthogonality between $f_{i\mu}^*$ and $\lambda_{ie}^{(1)}$:

$$(f_{1\mu}, f_{2\mu}) = \zeta(\lambda_{2e}^{(1)}, -\lambda_{1e}^{(1)})\,. \tag{5.11}$$

The contribution to a_μ then is proportional to

$$\lambda_{\mu 1}^{(1)\dagger} f_{1\mu}^* + \lambda_{\mu 2}^{(1)\dagger} f_{2\mu}^* = \zeta(\lambda_{2e}^{(1)*} \lambda_{1\mu}^{(1)*} - \lambda_{1e}^{(1)*} \lambda_{2\mu}^{(1)*})\,, \tag{5.12}$$

which is mostly fixed from neutrino parameters. The mass degeneracy $M_1 = M_2$ and the orthogonality condition (5.11) could in principle be justified by flavor symmetries [127] which needs much more structure and will not be treated here. This links the coupling f with λ so that all the terms in (4.7) scale as $1/v_1^2$. The vanishing (5.10) also makes the BSM contribution to electron EDM negligible, making it easily compatible with the current precise measurement [128, 129]. For the muon EDM, the combination (5.12) contributes but it is equally negligible compared to the current limit [130].

Considering now the complete contribution to the dipole coefficient $C_{\beta\alpha}^{\sigma R}$ in (4.7), the turning off (or suppression) of the electron coupling (5.10) eliminates the f^2 contribution (4.7c) for $\alpha = e$ or $\beta = e$. Analogously, the orthogonality condition (5.11) eliminates the mixed (left-right) contribution (4.7a), i.e., the chiral enhanced contribution, to the flavor transition $\mu \to e$ if N_1, N_2 have equal masses. Then, only the λ^2 term (left-left) in (4.7c), which is not enhanced, contributes to $\mu \to e\gamma$ while the chiral enhanced part still contributes dominantly to a_μ. With the increasing of the mass difference $\Delta M_N = M_2 - M_1$, the chiral enhanced contribution also increases rapidly for $\mu \to e\gamma$. In principle, we could change the orthogonality condition (5.11) to keep the chiral enhanced part (4.7a) vanishing, at the cost of devising a mass dependent condition. This vanishing could even be extended to the whole dipole coefficient (4.7). We will keep the simple orthogonality condition (5.11), and use the mass difference ΔM_N as a quantifier of the degree of tuning.

With the orthogonality condition, the couplings $f_{i\alpha}$ are completely determined by free variables related to neutrinos masses ($\mathrm{Im}(z)$, $M_1 = M_2 = M_N$), the vev v_1, and the scaling parameter ζ. Note that the real part of z is not physical for $M_1 = M_2$. Thus, for fixed
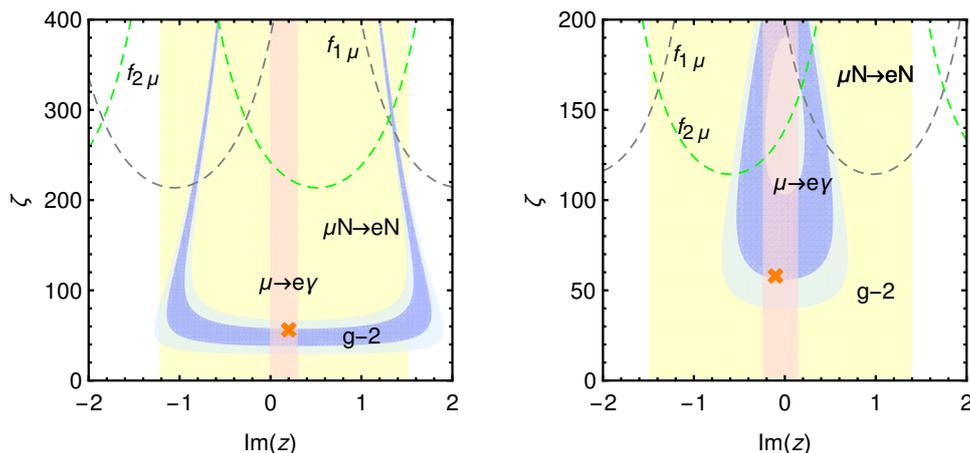
Figure 3. Allowed regions in the plane $\text{Im}(z) \times \zeta$ for NO (left) and IO (right). Scalar masses and s_γ are fixed as (5.13) while $M_N = 1\,\text{TeV}$ and $v_1 = x \times 10^{-3}\,\text{GeV}$ with $x = 1$ ($x = 2$) for NO (IO). The region above the gray (green) dashed lines are excluded by perturbativity on the couplings $f_{1\mu}$ ($f_{2\mu}$). The orange region is allowed by the present constraint on $\mu N \to eN$, while the light red region is related to $\mu \to e\gamma$. The dark (light) blue region show the 1(2)-σ region allowed by $(g-2)_\mu$. The crosses denote the benchmark points in (5.14). The mixing angles of the PMNS are fixed in best-fit of [131] whereas $\delta = 218°$.

values of M_N and v_1, we can impose perturbativity bounds $|f_{i\alpha}| < 4\pi$ as a function of $\text{Im}\, z$ and ζ. If the masses of the charged scalars and their mixing is also fixed, we can obtain further bounds by requiring compatibility with $(g-2)_\mu$ and $\mu \to e\gamma$. For both NO and IO, we choose

$$M_{S_1} = 350\,\text{GeV}, \quad M_{S_2} = 450\,\text{GeV}, \quad s_\gamma = 0.1. \tag{5.13}$$

Figure 3 shows allowed regions in the plane $\text{Im}(z) - \zeta$ for $(g-2)_\mu$ (blue), $\mu \to e\gamma$ (pink) and μe conversion in Au (yellow). Perturbativity for $f_{i\alpha}$ (dashed curves) is also shown. The left (right) figure is for NO (IO) for which $M_N = 1\,\text{TeV}$ and $v_1 = 10^{-3}\,\text{GeV}$ ($v_1 = 2 \times 10^{-3}\,\text{GeV}$). The mixing angles of the PMNS matrix are fixed in the best-fit of [131] while we choose $\delta = 218°$. Using a different value of δ leads to different shapes and regions for this plot and others that follow but the overall possibility of explaining $(g-2)_\mu$ and avoiding CLFV do not change significantly. The change is larger for NO. For IO the variation is not significant.

As illustrated in the plot, the strongest constraint on $\text{Im}(z)$ comes from $\mu \to e\gamma$. There is no visible constraint on ζ from $\mu \to e\gamma$ because the chiral enhanced term was chosen to vanish. The constraint on ζ will mainly come from $(g-2)_\mu$, whose dominant chiral enhanced contribution depends linearly on this variable. In turn, perturbativity bounds on f_{ij} impose upper bounds on ζ. For each NO and IO, we see that the following benchmark points account for $(g-2)_\mu$ still evading the current CLFV constraints:

$$\begin{aligned} \text{(BM-NO)} \quad & M_N = 1\,\text{TeV}, \quad v_1 = 10^{-3}\,\text{GeV}, \quad && z = 0.2i, \quad \zeta = 60; \\ \text{(BM-IO)} \quad & M_N = 1\,\text{TeV}, \quad v_1 = 2 \times 10^{-3}\,\text{GeV}, \quad && z = -0.1i, \quad \zeta = 60. \end{aligned} \tag{5.14}$$

Only v_1 and z differ in the two points. The rest of the model parameters are fixed as (5.13).
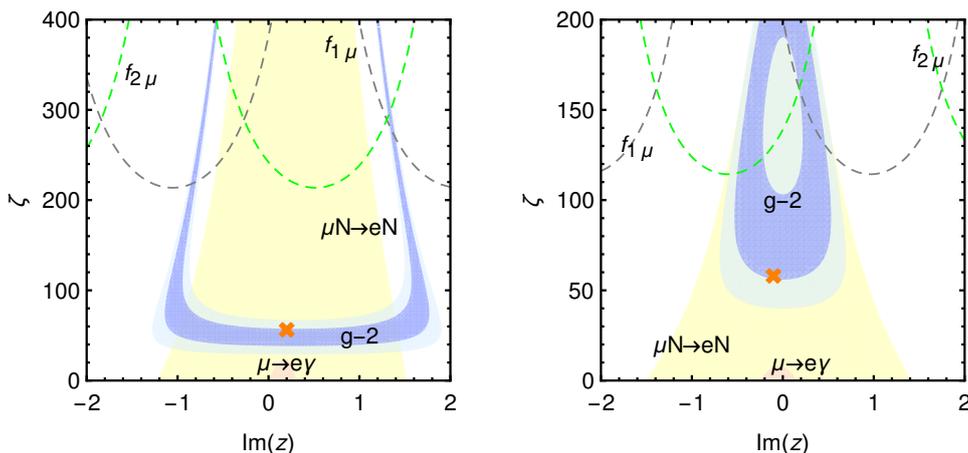
Figure 4. The same as figure 3, but for non-degenerate neutrino masses: $M_2 = 1.0001\,M_1$. Left: NO. Right: IO.

For comparison and to assess the degree of tuning, we show in figure 4 the allowed regions analogous to figure 3, with the same parameters, except for the lifting of the mass degeneracy of RHNs to $M_2 = 1.0001\,M_1$. We can see that we lose compatibiliy between $(g-2)_\mu$ at 1σ and $\mu \to e\gamma$ as the chiral enhanced term of the latter will not be completely canceled. The region of compatibility for $(g-2)_\mu$ is practically unchanged. We fix $\mathrm{Re}(z) = 0$ but we have checked that variation of $\mathrm{Re}(z)$ may lead at most to a difference of a factor two.

We illustrate in figures 5–7 the interplay of the distinct contributions to $g-2$, $\mu \to e\gamma$, and μe conversion in Au respectively, using the benchmarks defined in (5.13) and (5.14). In all the plots, we show the influence of the ζ parameter in the various contributions for each observable. Starting with the contributions to $g-2$, figure 5, we show that the chiral enhanced term given by (4.7a) is dominant, easily explaining the present anomaly. We also show in the figure that allowing for non-degenerate neutrino masses affects very little. Considering $\mu \to e\gamma$, for non-degenerate masses the chiral contribution can easily surpass the bound on $\mu \to e\gamma$. For the case of degenerate masses, the present bound can be avoided for this benchmark, even though for the future limit this would not be the case. The important point to notice is that all the contributions can be suppressed by increasing v_1 since all of them are proportional to v_1^{-2} under the orthogonality condition. However, since only the chiral contribution is proportional to $s_{2\gamma}$, we can still compensate by increasing the value of s_γ. This reasoning was applied when choosing the benchmark for IO, where v_1 is higher than the case for NO. At last, we comment on the present bounds on μe conversion in Au, figure 7. We show that the non-dipole contribution given by (4.19) is negligible compared to the dipole contribution given by (4.7). Moreover, as in the case of $\mu \to e\gamma$, if the neutrino masses are non-degenerate we can easily surpass the present bound.

To illustrate how the CLFV constraints are sensitive to the mass difference $M_2 - M_1$ of the RHNs, we can choose for NO the scaling $v_1 = 10^{-3}\,\mathrm{GeV}\sqrt{M_1/\mathrm{TeV}}$ such that the
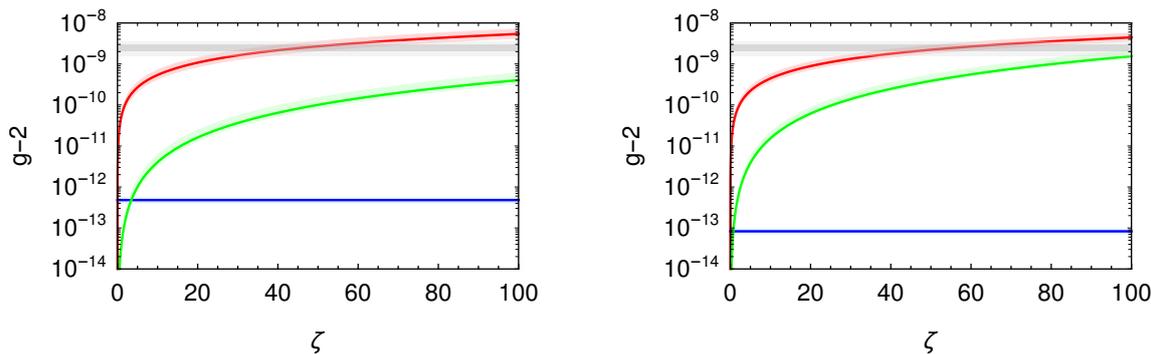
Figure 5. The absolute value of the contributions for $(g-2)_\mu$ as defined in eq. (4.7) as a function of ζ, for the benchmarks defined in (5.13) and (5.14) (left is NO and right is IO). The red line stands for the dominant chiral enhanced term (4.7a). The blue line refers to the λ^2 term, (4.7b), while the green line corresponds to the f^2 term, (4.7c). Both the green and blue contributions are negative, while the red one is positive. The dark (light) gray band corresponds to the $1(2)$-σ region allowed at present for $(g-2)_\mu$. The curves assumes $M_1 = M_2$ while the bands around them show the variation for $|M_2/M_1 - 1| \leq 0.4$.
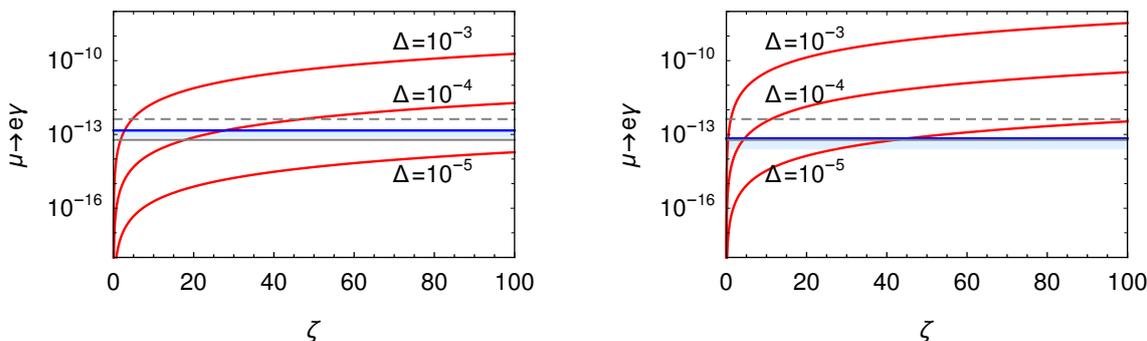
Figure 6. The contributions for $\mu \to e\gamma$ as defined in eq. (4.7) as a function of ζ, for the benchmarks defined in (5.13) and (5.14) (left is NO and right is IO). The red line stands for the chiral enhanced term (4.7a) while the blue line refers to the λ^2 term, cf. (4.7b). The dashed (continuous) gray line corresponds to the present (future) limits. Here, $\Delta = M_2/M_1 - 1$. The band around the blue line shows how much this contribution varies if Δ varies within $|\Delta| \leq 0.4$.

Yukawas $\lambda^{(1)}$ in (3.5) has the overall scale fixed as

$$(\lambda^{(1)}\lambda^{(1)\dagger})_{11} = \frac{M_1}{v_1^2}\Big(m_2|c_z|^2 + m_3|s_z|^2\Big) \sim 0.05 \times |s_z|^2\,, \qquad (5.15)$$

and the benchmark (5.14) is attained for $M_1 = 1\,\text{TeV}$. For the benchmark value we can see that $\lambda^{(1)} \sim O(0.1)$ and f is larger by ζ if respecting the orthogonality condition. For IO we choose twice the value for v_1 so that the benchmark (5.14) is also attained for $M_1 = 1\,\text{TeV}$.

We start with countour curves, shown in figure 8, for the current and future limit for $\mu \to e\gamma$ as a function of $\text{Im}(z)$ and M_1 for different values of $\Delta = M_2/M_1 - 1$. We clearly see that the curves move to the right as the mass difference increases showing that the constraints get stronger with the mass difference. The benchmark point, marked with a cross,
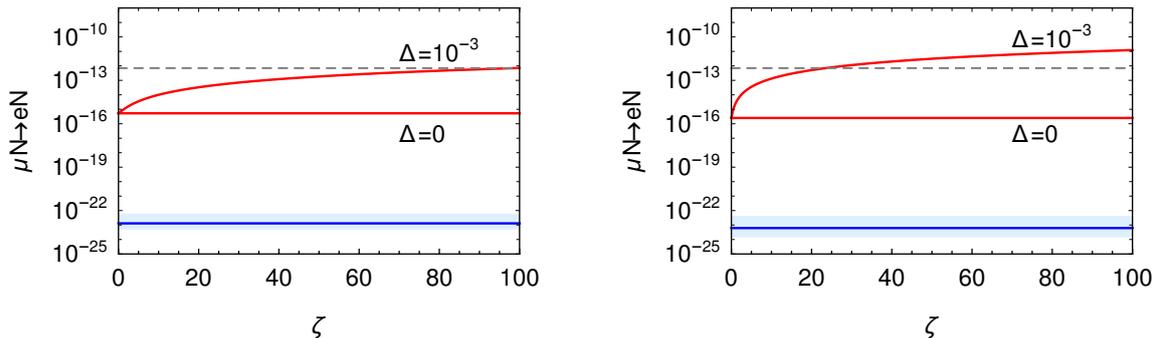
Figure 7. The contributions for Br(μAu→eAu) as defined in eqs. (4.7) and (4.19) as a function of ζ, for the benchmark defined in (5.13) and (5.14) (left is NO and right is IO). The red line stands for the dipole contribution (4.7), which is dominant. Moreover, if the neutrino masses are chosen non-degenerate, it can violate the present bound, given by the dashed gray line. The blue line is related to the non-dipole contribution, (4.19). Here, $\Delta = M_2/M_1 - 1$. The band around the blue line shows how much this contribution varies if Δ varies within $|\Delta| \leq 0.4$.
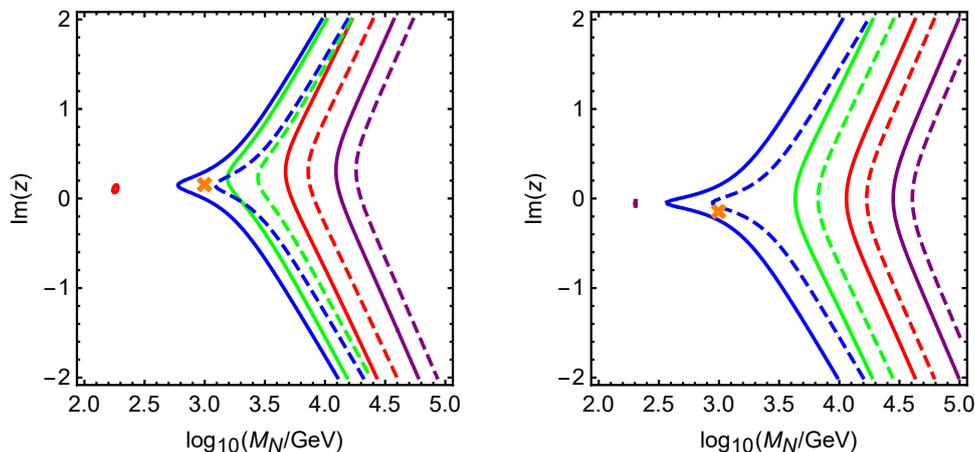
Figure 8. Contours for $\mu \to e\gamma$ for fixed $\zeta = 60$, and varying $M_2/M_1 - 1 = 0, 10^{-4}, 10^{-3}, 10^{-2}$ (respectively in blue, green, red and purple). The vev $v_1 = x \times 10^{-3}\,\mathrm{GeV}\sqrt{M_1/\mathrm{TeV}}$ scales with $\sqrt{M_1}$ so that the global scale for the Yukawa $\lambda^{(1)}$ is fixed. The continuous curves denote Br($\mu \to e\gamma$) = 4.2×10^{-13} (current) and the dashed ones denote Br($\mu \to e\gamma$) = 6×10^{-14} (future). The mass is $M_N = M_1$ and z is the parameter in (3.5) for NO (similarly for IO) with Re(z) = 0. Left: NO with $x = 1$. Right: IO with $x = 2$. The cross denotes the benchmark points defined in (5.13) and (5.14) for NO and IO.

is already excluded for $\Delta = 10^{-4}$ for both NO and IO. In the future, this benchmark will be excluded even for degenerate masses. A curve similar to the blue curve can be also found in ref. [99] where they consider the pure ν-2HDM without the charged singlet and hence equivalent to our case turning off $f_{j\alpha}$. The shape of the curve is not exactly the same because their treatment of the Casas-Ibarra parametrization of the minimal case is not appropriate. For certain curves, there are islands near $M_1 \sim 10^{2.3}\,\mathrm{GeV}$ indicating a destructive interference between the chiral enhanced contribution and the λ^2 contribution in (4.7).
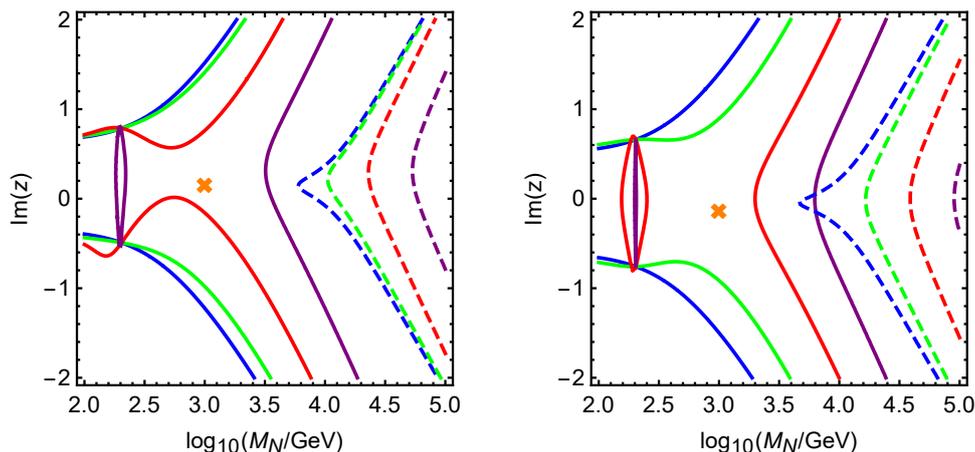
Figure 9. Contours for $\text{Br}(\mu N \to eN)$ for fixed $\zeta = 60$, and varying $M_2/M_1 - 1 = 0, 10^{-4}, 10^{-3}, 10^{-2}$ (respectively in blue, green, red and purple). The vev $v_1 = x \times 10^{-3}\,\text{GeV}\sqrt{M_1/\text{TeV}}$ scales with $\sqrt{M_1}$ so that the global scale for the Yukawa $\lambda^{(1)}$ is fixed. The continuous curves denote $N = \text{Au}$ (current) and the dashed denote $N = \text{Ti}$ (future). The mass is $M_N = M_1$ and z is the parameter in (3.5) for NO (similarly for IO) with $\text{Re}(z) = 0$. Left: NO with $x = 1$. Right: IO with $x = 2$. The cross denotes the benchmark points defined in (5.13) and (5.14) for NO and IO.

In figure 9, we show similar contours for μe conversion in nuclei. We can see that the future constraints will be much stronger than the current ones. Currently, a small mass difference is still allowed but in the future the benchmark will be easily excluded.

Finally we briefly comment on the dependence of our results on the masses of the charged scalars. The expression of the chiral enhanced contribution (4.7a) involves a cancellation between the contributions of the two charged scalars and it vanishes for degenerate masses. So up to a certain point, increasing the mass difference leads to an increase in the contribution to $g - 2$. This information can be seen in figure 10 where we show 1σ regions satisfying the $(g-2)_\mu$ constraint in the M_{S_1} and $M_N = M_1 = M_2$ plane keeping the ratio fixed as $M_{S_2}/M_{S_1} = 450/350 \approx 1.29$ (blue) and $M_{S_2}/M_{S_1} = 2$ (gray). We can see that the larger mass ratio allows a larger compatibility region with larger masses for the scalars and the RHNs. The benchmark points defined in (5.13) and (5.14) correspond to the origin of the plot in the corner of the blue region. Following this point to the right inside the blue region would still allow the compatibility to $(g-2)_\mu$ but with decreasing contribution to CLFV. We should remark that the mass difference of the charged scalars cannot be arbitrarily large as this would require an increasingly large μ_φ. The benchmark we have chosen, given by (5.13), is conservative in this sense, since it assumes $\mu_\varphi \sim -30$ GeV. For higher values, for instance, $-\mu_\varphi \sim$ TeV, it will still be possible to explain $(g-2)_\mu$ with masses of the charged scalars and the RHNs of $\mathcal{O}(\text{TeV})$ given all other parameters fixed as before. For even higher values of $-\mu_\varphi \sim 20$ TeV, we can avoid future constraints on μe conversion in nuclei and still satisfy $(g-2)_\mu$.

Before ending this section, let us briefly discuss the collider phenomenology. Given new particles with masses at the TeV scale, many BSM states can be searched for directly. Since the type IB seesaw model cannot account for $(g-2)_\mu$, we consider only the neutrinophilic
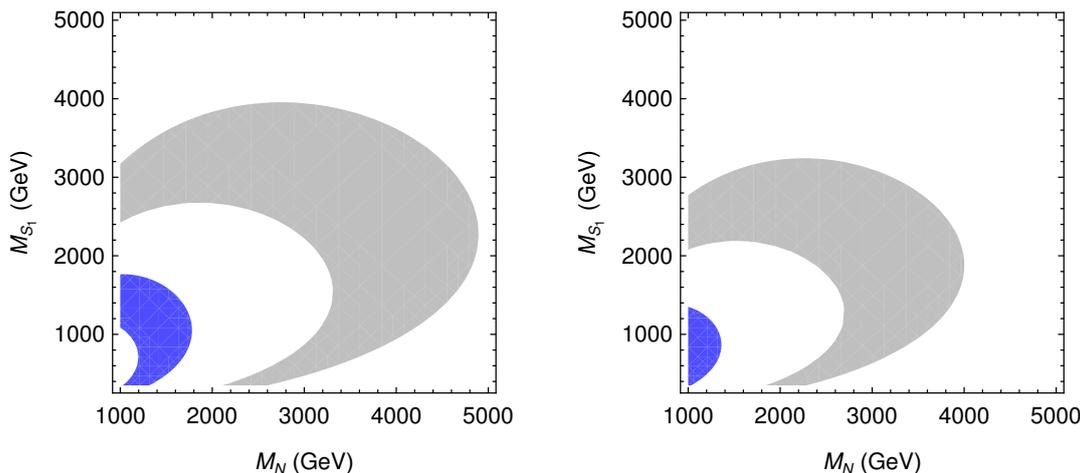
Figure 10. 1σ regions for $(g-2)_\mu$ in the M_{S_1} and $M_N = M_1 = M_2$ plane for fixed $\zeta = 60$, $s_\gamma = 0.1$ and two values of $M_{S_2}/M_{S_1} = 450/350 \approx 1.29$ (blue) and $M_{S_2}/M_{S_1} = 2$ (gray). The vev $v_1 = x \times 10^{-3}\,\text{GeV}\,\sqrt{M_1/\text{TeV}}$ scales with $\sqrt{M_1}$ so that the global scale for the Yukawa $\lambda^{(1)}$ is fixed. Left: NO with $x = 1$ and z as in (5.14). Right: IO with $x = 2$ and z as in (5.14).

version in eq. (2.3) in which the neutrinophilic Higgs doublet $\Phi_1 \sim H_\nu$ essentially contains only BSM states and their interactions with quarks are suppressed by the large $\tan\beta$, just as in the type I 2HDM. The interaction with quarks of the charged scalars within the singlet φ^+ are analogously suppressed and occurs only through mixing. Therefore, the dominant production mechanism at LHC for the charged scalars present in the extended neutrinophilic model will be through pair production $q\bar{q} \to \gamma^*(Z^*) \to S^- S^+$ [132, 133], while the production of the gauge singlets N_R will be highly suppressed [134] by the light-heavy neutrino mixing $|V_{\ell N}| \sim v_1 \lambda^{(1)}/M_N \sim 10^{-6}$ for $M_N \sim$ TeV and $v_1 \sim$ MeV. Therefore, we will not consider the decay of N_R.

The decay mode of the charged scalars S_i^+ depends on their masses relative to the masses of the RHNs. If $M_{S_i} < M_{N_j}$, assumed in our benchmarks, and not so large $\tan\beta = v_2/v_1$, the decay of S_i occurs dominantly through the Yukawa coupling to Φ_2, which contains a tiny admixture of S_i^+. The dominant width to tb quarks is roughly

$$\Gamma(S_i^+ \to tb) \sim \frac{y_t^2}{\tan^2\beta}\frac{M_{H^\pm}}{16\pi}\,, \tag{5.16}$$

where we ignore the suppression by c_γ^2 or s_γ^2. For large $\tan\beta$, the dominant decay is through Yukawa couplings $\lambda^{(1)}$ and f suppressed by the small mixing between the light and heavy neutrinos with width

$$\Gamma(S_i^+ \to \ell_\alpha^+ \nu_j) \approx \frac{M_{S_i}}{16\pi}\left[|\Gamma_{j\alpha}^H a_i|^2 + |\Gamma_{j\alpha}^\varphi b_i|^2\right]\,, \tag{5.17}$$

where $\Gamma^H = v_1 V^\mathsf{T}\lambda^{(1)\mathsf{T}} M_R^{-1}\lambda^{(1)} = \hat{M}_\nu V^\dagger/v_1$, $\Gamma^\varphi = v_1 V^\dagger \lambda^{(1)\dagger} M_R^{-1} f^*$, $(a_1, a_2) = (c_\gamma, -s_\gamma)$, $(b_1, b_2) = (s_\gamma, c_\gamma)$. The term with Γ^H is already present in the ν-2HDM without the charged singlet [97, 98]. As we need $f_{1\mu}, f_{2\mu} \sim O(1)$ to solve $(g-2)_\mu$, the contribution from Γ^φ

is larger. From a rough estimate, the decay (5.17) start to dominate for $\tan\beta \gtrsim 10^6$. In contrast, if $M_{S_i} > M_{N_j}$, the charged scalars decay rapidly through the Yukawa couplings $\lambda^{(1)}$ and f into charged leptons and N_R. The latter will be long-lived and decay to $W^+\ell_\alpha$ or $Z\nu_j$ with rates suppressed by the light-heavy neutrino mixing.

To conclude this section, we have seen that the solution for $(g-2)_\mu$ within our model requires a sensitive balance of parameters to evade the strong bounds coming from CLFV processes. In general, increasing s_γ, increasing $f_{j\alpha}$ or decreasing v_1 will increase the chiral enhanced contribution which dominates in $(g-2)_\mu$ but also in the CLFV processes if not properly suppressed.

6 Summary

In order to connect the mechanism of neutrino mass generation with the $(g-2)_\mu$ anomaly, we proposed to add a single charged singlet to the neutrinophilic 2HDM and a variant which implements a low scale seesaw by attributing part of the smallness of neutrino masses to a small vev. We studied two models: (a) the ν-2HDM version and (b) the type IB seesaw version, both for the minimal case of two righthanded neutrinos. A chiral enhanced contribution to $(g-2)_\mu$ is generated through exchange of charged scalars and righthanded neutrinos, the latter also participating in the neutrino mass generation. As family lepton number breaking is also brought to low scale, the chiral enhanced contribution generically leads to large rates for CLFV processes. We find that the type IB seesaw implementation does not have enough freedom to circumvent the constraints from CLFV while solving the $(g-2)_\mu$ anomaly. The ν-2HDM version, on the other hand, has enough freedom to allow some special cases where $(g-2)_\mu$ anomaly can be solved and yet avoiding the stringent CLFV processes. Even in these special cases, the region of compatibility between $(g-2)_\mu$ and current CLFV is very restricted. One region for some choices of parameters is given in figure 3. It is clear that our solutions are not restricted to the minimal case of two RHNs as this limit can be mimicked in the presence of three righthanded neutrinos and more regions may open up. In the future, experiments of μe conversion in different nuclei are expected to drastically improve the limits and this kind of solution to the $(g-2)_\mu$ anomaly will be put to test.

A Wilson coefficients

Here we describe briefly how we obtain the Wilson coefficients of the effective photonic operators (4.1). The calculations are based on appendices B and C.

A.1 ν-2HDM model

For the dipole part, the contribution (4.7b) comes from the LL part of the penguin diagram leading to (B.2a) with the following couplings multiplying (C.1):

$$N_k - S_1^+ : \quad - e\lambda_{\beta k}^{(1)\dagger} \frac{v_2 c_\gamma}{v} \lambda_{k\alpha}^{(1)} \frac{v_2 c_\gamma}{v} ,$$
$$N_k - S_2^+ : \quad - e\lambda_{\beta k}^{(1)\dagger} \frac{v_2(-s_\gamma)}{v} \lambda_{k\alpha}^{(1)} \frac{v_2(-s_\gamma)}{v} . \tag{A.1}$$

The masses should be attributed accordingly. The contribution (4.7c) comes from the RR part of the penguin diagram leading to (B.2a), L-R exchanged, with the following couplings multiplying (C.2):

$$N_k - S_1^+ : \quad - e f_{\beta k}^{\mathsf{T}} s_\gamma f_{k\alpha}^* s_\gamma ,$$
$$N_k - S_2^+ : \quad - e f_{\beta k}^{\mathsf{T}} c_\gamma f_{k\alpha}^* c_\gamma . \tag{A.2}$$

The chirally enhanced contribution (4.7a) comes from LR part of the penguin diagram leading to (B.2b), with the following couplings multiplying (C.4):

$$N_k - S_1^+ : \quad - e\lambda_{\beta k}^{(1)\dagger} \frac{v_2 c_\gamma}{v} f_{k\alpha}^* s_\gamma ,$$
$$N_k - S_2^+ : \quad - e\lambda_{\beta k}^{(1)\dagger} \frac{v_2(-s_\gamma)}{v} f_{k\alpha}^* c_\gamma . \tag{A.3}$$

For the non-dipole part, there are only chirality preserving contributions. The integral I_{LL}^μ (B.2a) and the coefficient (C.3) should be multiplied by (A.1) while the analogous I_{RR}^μ should be multiplied by (A.2), resulting in the coefficients (4.19).

A.2 Seesaw type IB

The contribution (4.12b) comes from the LL part (B.2a) with the following couplings multiplying (C.1):

$$N - S_1^+ : \quad - e\lambda_{\beta 1}^\dagger \frac{v_2 c_\gamma}{v} \lambda_{1\alpha} \frac{v_2 c_\gamma}{v} ,$$
$$N - S_2^+ : \quad - e\lambda_{\beta 1}^\dagger \frac{v_2(-s_\gamma)}{v} \lambda_{1\alpha} \frac{v_2(-s_\gamma)}{v} . \tag{A.4}$$

The contribution (4.12c) comes from the RR part of (B.2a), L-R exchanged, with the following couplings multiplying (C.2):

$$N - S_1^+ : \quad - e f_{\beta 2}^{\mathsf{T}} s_\gamma f_{2\alpha}^* s_\gamma ,$$
$$N - S_2^+ : \quad - e f_{\beta 2}^{\mathsf{T}} c_\gamma f_{2\alpha}^* c_\gamma . \tag{A.5}$$

The chirally enhanced contribution (4.12a) comes from LR part of the penguin diagram leading to (B.2b), with the following couplings multiplying (C.4):

$$N - S_1^+ : \quad - e\lambda_{\beta 1}^\dagger \frac{v_2}{v} c_\gamma f_{2\alpha}^* s_\gamma ,$$
$$N - S_2^+ : \quad - e\lambda_{\beta 1}^\dagger \frac{v_2}{v} (-s_\gamma) f_{2\alpha}^* c_\gamma . \tag{A.6}$$

Other combinations are forbidden by the pseudo-Dirac nature of N.

For the non-dipole part, there are only chirality preserving contributions. The integral I_{LL}^μ (B.2a) and the coefficient (C.3) should be multiplied by (A.1) while the analogous I_{RR}^μ should be multiplied by (A.2), resulting in the coefficients (4.21).

B Loop integrals

Our calculations for loop integrals and operators are similar to refs. [135, 136]. The following loop integrals come from self-energy diagrams and penguin diagrams in figure 2:

$$iI_{LL} = \int \frac{d^4k}{(2\pi)^4} \frac{R\slashed{k}}{(k^2 - M_N^2)[(k-p)^2 - M_\varphi^2]}$$
$$= \frac{iR}{(4\pi)^2} \frac{\slashed{p}}{2} \left\{ \frac{1}{\epsilon} + \log \frac{\bar{\mu}^2}{M_\varphi^2} + h_S(x) + \frac{p^2}{M_\varphi^2} 8\tilde{f}_S(x) \right\} , \quad \text{(B.1a)}$$

$$iI_{LR} = \int \frac{d^4k}{(2\pi)^4} \frac{RM_N}{(k^2 - M_N^2)[(k-p)^2 - M_\varphi^2]}$$
$$= \frac{iR}{(4\pi)^2} M_N \left\{ \frac{1}{\epsilon} + \log \frac{\bar{\mu}^2}{M_\varphi^2} + \frac{1 - x + x\log x}{1 - x} + \frac{p^2}{M_\varphi^2} 2f_S(x) \right\} , \quad \text{(B.1b)}$$

$$iI_{LL}^\mu = \int \frac{d^4k}{(2\pi)^4} \frac{R\slashed{k}(p_1 + p_2 - 2k)^\mu}{(k^2 - M_N^2)[(k-p_1)^2 - M_\varphi^2][(k-p_2)^2 - M_\varphi^2]}$$
$$= -\frac{iR}{(4\pi)^2} \left\{ \frac{1}{2} \gamma^\mu \left[\frac{1}{\epsilon} + \log \frac{\bar{\mu}^2}{M_\varphi^2} + h_S(x) \right] + \frac{1}{M_\varphi^2} (q^2 \gamma^\mu - \slashed{q}q^\mu) \frac{1}{6} G_S(x) \right.$$
$$\left. + \frac{1}{M_\varphi^2} [(\slashed{p}_1 + \slashed{p}_2)(p_1 + p_2)^\mu + (p_1^2 + p_2^2)\gamma^\mu] 2\tilde{f}_S(x) \right\} , \quad \text{(B.2a)}$$

$$iI_{LR}^\mu = \int \frac{d^4k}{(2\pi)^4} \frac{RM_N(p_1 + p_2 - 2k)^\mu}{(k^2 - M_N^2)[(k-p_1)^2 - M_\varphi^2][(k-p_2)^2 - M_\varphi^2]}$$
$$= -\frac{iR}{(4\pi)^2} \frac{M_N}{M_\varphi^2} (p_1 + p_2)^\mu 2f_S(x) , \quad \text{(B.2b)}$$

where $x = M_N^2/M_\varphi^2$ and $q = p_2 - p_1$. These expression should be supplied with couplings and enclosed by spinors $\bar{u}(p_2)$ and $u(p_1)$ to give the amplitudes. Simple chirality exchange $L \leftrightarrow R$ leads to identical expressions with the projector exchanged. We use dimensional regularization with $d = 4 - 2\epsilon$ and retain only terms up to M_φ^{-2} or M_N^{-2}. The additional loop function that appear is

$$h_S(x) = \frac{1 - 4x + 3x^2 - 2x^2 \log x}{2(1 - x)^2} . \quad \text{(B.3)}$$

The result for I_{LL} and I_{LL}^μ match [135] for $x \to 0$ as $8\tilde{f}_S(0) = 1/3$ and $G_S(0) = 1/3$.

For the last integral in (B.2b), we can use the Gordon-type identity where we can replace

$$(p_1 + p_2)^\mu \to -i\sigma^{\mu\nu} q_\nu + \slashed{p}_2 \gamma^\mu + \gamma^\mu \slashed{p}_1 . \quad \text{(B.4)}$$

C Operators

The operators relevant to CLFV are the photon interactions written in (4.1). The operator in the first line is the dipole contribution whereas the ones in the second line are the non-dipole (ND) part. These Wilson coefficients at 1-loop can be obtained by matching the

full theory with the effective theory through appropriate 1-loop amplitudes. The relevant amplitudes lead to the expressions in (B.1) and (B.2) which comes from the self-energy and dipole diagrams in figure 2. To obtain the full expressions, one only needs to add the coupling constants and adapt the masses.

Let us focus first on the chirality preserving contributions. The coefficient of $\not{p}$ in (B.1a) and of the γ^μ part in (B.2a) give rise to the operator $\bar{\psi}_L \not{D} \psi_L$, ψ being the collection of lepton fields, and it should be removed by wave function renormalization. The coefficient of $\not{p}p^2$ in (B.1a) and the last term in the square brackets in (B.2a) lead to the operator $\bar{\psi}_L (\not{D} D^2 + D^2 \not{D}) \psi_L$ [135]. This operator can be replaced by $\bar{\psi}_L \not{D}^3 \psi_L$ with additional dipole contributions. The former operator does not lead to relevant physical phenomena. The result is that the last term in I_{LL}^μ (B.2a) generates

$$\delta C_{\beta\alpha}^{\sigma R} = \frac{(-1)}{(4\pi)^2} \frac{1}{2M_\varphi^2} 2\tilde{f}_S(x) m_\alpha \,, \tag{C.1}$$

while an analogous I_{RR}^μ leads to

$$\delta C_{\beta\alpha}^{\sigma R} = m_\beta \frac{(-1)}{(4\pi)^2} \frac{1}{2M_\varphi^2} 2\tilde{f}_S(x) \,. \tag{C.2}$$

These contributions are chirality flipping after the use of the equations of motion. Finally, the contribution proportional to $G_S(x)$ in (B.2a) leads to the non-dipole term with

$$C_{\beta\alpha}^{\text{ND-}L} = \frac{(-1)}{(4\pi)^2} \frac{1}{6M_\varphi^2} G_S(x) \,. \tag{C.3}$$

A similar term comes from I_{RR}^μ.

Let us now turn to the chirality flipping contributions. The coefficient of M_N in (B.1b) should be removed by lepton mass renormalization. The coefficient of $p^2 M_N$ in (B.1b) and the coefficient of $\not{p}_2 \gamma^\mu + \gamma^\mu \not{p}_1$ in (B.2b), after replacement (B.4), leads to the operator $\bar{\psi}_L \not{D}^2 \psi_R$ which is not phenomenologically relevant. The dipole contribution (B.4) in (B.2b) leads to

$$\delta C_{\alpha\beta}^{\sigma R} = \frac{1}{(4\pi)^2} \frac{M_N}{M_\varphi^2} 2 f_S(x) \,. \tag{C.4}$$

References

[1] T. Ohlsson, *Special issue on "neutrino oscillations: celebrating the Nobel prize in physics 2015" in Nuclear Physics B*, *Nucl. Phys. B* **908** (2016) 1.

[2] S. Weinberg, *Baryon and lepton nonconserving processes*, *Phys. Rev. Lett.* **43** (1979) 1566 [INSPIRE].

[3] MUON G-2 collaboration, *Measurement of the positive muon anomalous magnetic moment to* 0.46 *ppm*, *Phys. Rev. Lett.* **126** (2021) 141801 [arXiv:2104.03281] [INSPIRE].

[4] Muon g-2 collaboration, *Measurement of the positive muon anomalous magnetic moment to* 0.20 *ppm*, arXiv:2308.06230 [inSPIRE].

[5] T. Aoyama et al., *The anomalous magnetic moment of the muon in the Standard Model*, *Phys. Rept.* **887** (2020) 1 [arXiv:2006.04822] [inSPIRE].

[6] T. Aoyama, M. Hayakawa, T. Kinoshita and M. Nio, *Complete tenth-order QED contribution to the muon g − 2*, *Phys. Rev. Lett.* **109** (2012) 111808 [arXiv:1205.5370] [inSPIRE].

[7] T. Aoyama, T. Kinoshita and M. Nio, *Theory of the anomalous magnetic moment of the electron*, *Atoms* **7** (2019) 28 [inSPIRE].

[8] A. Czarnecki, W.J. Marciano and A. Vainshtein, *Refinements in electroweak contributions to the muon anomalous magnetic moment*, *Phys. Rev. D* **67** (2003) 073006 [*Erratum ibid.* **73** (2006) 119901] [hep-ph/0212229] [inSPIRE].

[9] C. Gnendiger, D. Stöckinger and H. Stöckinger-Kim, *The electroweak contributions to* $(g − 2)_\mu$ *after the Higgs boson mass measurement*, *Phys. Rev. D* **88** (2013) 053005 [arXiv:1306.5546] [inSPIRE].

[10] M. Davier, A. Hoecker, B. Malaescu and Z. Zhang, *Reevaluation of the hadronic vacuum polarisation contributions to the Standard Model predictions of the muon g − 2 and* $\alpha(m_Z^2)$ *using newest hadronic cross-section data*, *Eur. Phys. J. C* **77** (2017) 827 [arXiv:1706.09436] [inSPIRE].

[11] A. Keshavarzi, D. Nomura and T. Teubner, *Muon g − 2 and* $\alpha(M_Z^2)$: *a new data-based analysis*, *Phys. Rev. D* **97** (2018) 114025 [arXiv:1802.02995] [inSPIRE].

[12] G. Colangelo, M. Hoferichter and P. Stoffer, *Two-pion contribution to hadronic vacuum polarization*, *JHEP* **02** (2019) 006 [arXiv:1810.00007] [inSPIRE].

[13] M. Hoferichter, B.-L. Hoid and B. Kubis, *Three-pion contribution to hadronic vacuum polarization*, *JHEP* **08** (2019) 137 [arXiv:1907.01556] [inSPIRE].

[14] M. Davier, A. Hoecker, B. Malaescu and Z. Zhang, *A new evaluation of the hadronic vacuum polarisation contributions to the muon anomalous magnetic moment and to* $\alpha(m_Z^2)$, *Eur. Phys. J. C* **80** (2020) 241 [*Erratum ibid.* **80** (2020) 410] [arXiv:1908.00921] [inSPIRE].

[15] A. Keshavarzi, D. Nomura and T. Teubner, *g − 2 of charged leptons,* $\alpha(M_Z^2)$, *and the hyperfine splitting of muonium*, *Phys. Rev. D* **101** (2020) 014029 [arXiv:1911.00367] [inSPIRE].

[16] A. Kurz, T. Liu, P. Marquard and M. Steinhauser, *Hadronic contribution to the muon anomalous magnetic moment to next-to-next-to-leading order*, *Phys. Lett. B* **734** (2014) 144 [arXiv:1403.6400] [inSPIRE].

[17] K. Melnikov and A. Vainshtein, *Hadronic light-by-light scattering contribution to the muon anomalous magnetic moment revisited*, *Phys. Rev. D* **70** (2004) 113006 [hep-ph/0312226] [inSPIRE].

[18] P. Masjuan and P. Sanchez-Puertas, *Pseudoscalar-pole contribution to the* $(g_\mu − 2)$: *a rational approach*, *Phys. Rev. D* **95** (2017) 054026 [arXiv:1701.05829] [inSPIRE].

[19] G. Colangelo, M. Hoferichter, M. Procura and P. Stoffer, *Dispersion relation for hadronic light-by-light scattering: two-pion contributions*, *JHEP* **04** (2017) 161 [arXiv:1702.07347] [inSPIRE].

[20] M. Hoferichter et al., *Dispersion relation for hadronic light-by-light scattering: pion pole*, *JHEP* **10** (2018) 141 [`arXiv:1808.04823`] [InSPIRE].

[21] A. Gérardin, H.B. Meyer and A. Nyffeler, *Lattice calculation of the pion transition form factor with $N_f = 2 + 1$ Wilson quarks*, *Phys. Rev. D* **100** (2019) 034520 [`arXiv:1903.09471`] [InSPIRE].

[22] J. Bijnens, N. Hermansson-Truedsson and A. Rodríguez-Sánchez, *Short-distance constraints for the HLbL contribution to the muon anomalous magnetic moment*, *Phys. Lett. B* **798** (2019) 134994 [`arXiv:1908.03331`] [InSPIRE].

[23] G. Colangelo et al., *Longitudinal short-distance constraints for the hadronic light-by-light contribution to $(g-2)_\mu$ with large-N_c Regge models*, *JHEP* **03** (2020) 101 [`arXiv:1910.13432`] [InSPIRE].

[24] T. Blum et al., *Hadronic light-by-light scattering contribution to the muon anomalous magnetic moment from lattice QCD*, *Phys. Rev. Lett.* **124** (2020) 132002 [`arXiv:1911.08123`] [InSPIRE].

[25] G. Colangelo et al., *Remarks on higher-order hadronic corrections to the muon $g-2$*, *Phys. Lett. B* **735** (2014) 90 [`arXiv:1403.7512`] [InSPIRE].

[26] S. Borsanyi et al., *Leading hadronic contribution to the muon magnetic moment from lattice QCD*, *Nature* **593** (2021) 51 [`arXiv:2002.12347`] [InSPIRE].

[27] FERMILAB LATTICE et al. collaborations, *Light-quark connected intermediate-window contributions to the muon $g-2$ hadronic vacuum polarization from lattice QCD*, *Phys. Rev. D* **107** (2023) 114514 [`arXiv:2301.08274`] [InSPIRE].

[28] T. Blum et al., *An update of Euclidean windows of the hadronic vacuum polarization*, [`arXiv:2301.08696`] [InSPIRE].

[29] EXTENDED TWISTED MASS collaboration, *Lattice calculation of the short and intermediate time-distance hadronic vacuum polarization contributions to the muon magnetic moment using twisted-mass fermions*, *Phys. Rev. D* **107** (2023) 074506 [`arXiv:2206.15084`] [InSPIRE].

[30] M. Cè et al., *Window observable for the hadronic vacuum polarization contribution to the muon $g-2$ from lattice QCD*, *Phys. Rev. D* **106** (2022) 114502 [`arXiv:2206.06582`] [InSPIRE].

[31] C. Aubin, T. Blum, M. Golterman and S. Peris, *Muon anomalous magnetic moment with staggered fermions: is the lattice spacing small enough?*, *Phys. Rev. D* **106** (2022) 054503 [`arXiv:2204.12256`] [InSPIRE].

[32] CHIQCD collaboration, *Muon $g-2$ with overlap valence fermions*, *Phys. Rev. D* **107** (2023) 034513 [`arXiv:2204.01280`] [InSPIRE].

[33] C. Lehner and A.S. Meyer, *Consistency of hadronic vacuum polarization between lattice QCD and the R-ratio*, *Phys. Rev. D* **101** (2020) 074515 [`arXiv:2003.04177`] [InSPIRE].

[34] G. Colangelo et al., *Data-driven evaluations of Euclidean windows to scrutinize hadronic vacuum polarization*, *Phys. Lett. B* **833** (2022) 137313 [`arXiv:2205.12963`] [InSPIRE].

[35] K. Kannike, M. Raidal, D.M. Straub and A. Strumia, *Anthropic solution to the magnetic muon anomaly: the charged see-saw*, *JHEP* **02** (2012) 106 [*Erratum ibid.* **10** (2012) 136] [`arXiv:1111.2551`] [InSPIRE].

[36] A. Freitas, J. Lykken, S. Kell and S. Westhoff, *Testing the muon $g − 2$ anomaly at the LHC*, *JHEP* **05** (2014) 145 [*Erratum ibid.* **09** (2014) 155] [arXiv:1402.7065] [INSPIRE].

[37] A. Crivellin, M. Hoferichter and P. Schmidt-Wellenburg, *Combined explanations of $(g − 2)_{\mu,e}$ and implications for a large muon EDM*, *Phys. Rev. D* **98** (2018) 113002 [arXiv:1807.11484] [INSPIRE].

[38] L. Calibbi, R. Ziegler and J. Zupan, *Minimal models for dark matter and the muon $g − 2$ anomaly*, *JHEP* **07** (2018) 046 [arXiv:1804.00009] [INSPIRE].

[39] P. Athron et al., *New physics explanations of a_μ in light of the FNAL muon $g − 2$ measurement*, *JHEP* **09** (2021) 080 [arXiv:2104.03691] [INSPIRE].

[40] M. Lindner, M. Platscher and F.S. Queiroz, *A call for new physics: the muon anomalous magnetic moment and lepton flavor violation*, *Phys. Rept.* **731** (2018) 1 [arXiv:1610.06587] [INSPIRE].

[41] R. Capdevilla, D. Curtin, Y. Kahn and G. Krnjaic, *No-lose theorem for discovering the new physics of $(g − 2)_\mu$ at muon colliders*, *Phys. Rev. D* **105** (2022) 015028 [arXiv:2101.10334] [INSPIRE].

[42] W. Yin and M. Yamaguchi, *Muon $g − 2$ at a multi-TeV muon collider*, *Phys. Rev. D* **106** (2022) 033007 [arXiv:2012.03928] [INSPIRE].

[43] K.S. Babu, S. Jana, M. Lindner and V.P. K, *Muon $g − 2$ anomaly and neutrino magnetic moments*, *JHEP* **10** (2021) 240 [arXiv:2104.03291] [INSPIRE].

[44] G. Mohlabeng, *Revisiting the dark photon explanation of the muon anomalous magnetic moment*, *Phys. Rev. D* **99** (2019) 115001 [arXiv:1902.05075] [INSPIRE].

[45] D.W.P. Amaral, D.G. Cerdeno, A. Cheek and P. Foldenauer, *Confirming* $U(1)_{L_\mu − L_\tau}$ *as a solution for $(g − 2)_\mu$ with neutrinos*, *Eur. Phys. J. C* **81** (2021) 861 [arXiv:2104.03297] [INSPIRE].

[46] C. Arbeláez, R. Cepedello, R.M. Fonseca and M. Hirsch, *$(g − 2)$ anomalies and neutrino mass*, *Phys. Rev. D* **102** (2020) 075005 [arXiv:2007.11007] [INSPIRE].

[47] I. Bigaran and R.R. Volkas, *Getting chirality right: single scalar leptoquark solutions to the $(g − 2)_{e,\mu}$ puzzle*, *Phys. Rev. D* **102** (2020) 075037 [arXiv:2002.12544] [INSPIRE].

[48] I. Doršner, S. Fajfer and S. Saad, *$\mu \to e\gamma$ selecting scalar leptoquark solutions for the $(g − 2)_{e,\mu}$ puzzles*, *Phys. Rev. D* **102** (2020) 075007 [arXiv:2006.11624] [INSPIRE].

[49] D. Zhang, *Radiative neutrino masses, lepton flavor mixing and muon $g − 2$ in a leptoquark model*, *JHEP* **07** (2021) 069 [arXiv:2105.08670] [INSPIRE].

[50] R. Dermisek and A. Raval, *Explanation of the muon $g − 2$ anomaly with vectorlike leptons and its implications for Higgs decays*, *Phys. Rev. D* **88** (2013) 013017 [arXiv:1305.3522] [INSPIRE].

[51] R. Dermisek, K. Hermanek, N. McGinnis and N. McGinnis, *Highly enhanced contributions of heavy Higgs bosons and new leptons to muon $g − 2$ and prospects at future colliders*, *Phys. Rev. Lett.* **126** (2021) 191801 [arXiv:2011.11812] [INSPIRE].

[52] A. Broggio et al., *Limiting two-Higgs-doublet models*, *JHEP* **11** (2014) 058 [arXiv:1409.3199] [INSPIRE].

[53] V. Ilisie, *New Barr-Zee contributions to $(g − 2)_\mu$ in two-Higgs-doublet models*, *JHEP* **04** (2015) 077 [arXiv:1502.04199] [INSPIRE].

[54] T. Han, S.K. Kang and J. Sayre, *Muon g − 2 in the aligned two Higgs doublet model*, *JHEP* **02** (2016) 097 [arXiv:1511.05162] [INSPIRE].

[55] A. Cherchiglia, P. Kneschke, D. Stöckinger and H. Stöckinger-Kim, *The muon magnetic moment in the 2HDM: complete two-loop result*, *JHEP* **01** (2017) 007 [*Erratum ibid.* **10** (2021) 242] [arXiv:1607.06292] [INSPIRE].

[56] A. Cherchiglia, D. Stöckinger and H. Stöckinger-Kim, *Muon g − 2 in the 2HDM: maximum results and detailed phenomenology*, *Phys. Rev. D* **98** (2018) 035001 [arXiv:1711.11567] [INSPIRE].

[57] T. Abe, R. Sato and K. Yagyu, *Muon specific two-Higgs-doublet model*, *JHEP* **07** (2017) 012 [arXiv:1705.01469] [INSPIRE].

[58] D. Stockinger, *The muon magnetic moment and supersymmetry*, *J. Phys. G* **34** (2007) R45 [hep-ph/0609168] [INSPIRE].

[59] M. Endo and W. Yin, *Explaining electron and muon g − 2 anomaly in SUSY without lepton-flavor mixings*, *JHEP* **08** (2019) 122 [arXiv:1906.08768] [INSPIRE].

[60] J. Hisano and K. Tobe, *Neutrino masses, muon g − 2, and lepton flavor violation in the supersymmetric seesaw model*, *Phys. Lett. B* **510** (2001) 197 [hep-ph/0102315] [INSPIRE].

[61] P. Minkowski, *μ → eγ at a rate of one out of 10^9 muon decays?*, *Phys. Lett. B* **67** (1977) 421 [INSPIRE].

[62] M. Gell-Mann, P. Ramond and R. Slansky, *Complex spinors and unified theories*, *Conf. Proc. C* **790927** (1979) 315 [arXiv:1306.4669] [INSPIRE].

[63] R.N. Mohapatra and G. Senjanovic, *Neutrino mass and spontaneous parity nonconservation*, *Phys. Rev. Lett.* **44** (1980) 912 [INSPIRE].

[64] M. Magg and C. Wetterich, *Neutrino mass problem and gauge hierarchy*, *Phys. Lett. B* **94** (1980) 61 [INSPIRE].

[65] J. Schechter and J.W.F. Valle, *Neutrino masses in SU(2) × U(1) theories*, *Phys. Rev. D* **22** (1980) 2227 [INSPIRE].

[66] G. Lazarides, Q. Shafi and C. Wetterich, *Proton lifetime and fermion masses in an SO(10) model*, *Nucl. Phys. B* **181** (1981) 287 [INSPIRE].

[67] R.N. Mohapatra and G. Senjanovic, *Neutrino masses and mixings in gauge models with spontaneous parity violation*, *Phys. Rev. D* **23** (1981) 165 [INSPIRE].

[68] E. Ma and U. Sarkar, *Neutrino masses and leptogenesis with heavy Higgs triplets*, *Phys. Rev. Lett.* **80** (1998) 5716 [hep-ph/9802445] [INSPIRE].

[69] R. Foot, H. Lew, X.G. He and G.C. Joshi, *Seesaw neutrino masses induced by a triplet of leptons*, *Z. Phys. C* **44** (1989) 441 [INSPIRE].

[70] E. Ma, *Pathways to naturally small neutrino masses*, *Phys. Rev. Lett.* **81** (1998) 1171 [hep-ph/9805219] [INSPIRE].

[71] E. Ma and D.P. Roy, *Heavy triplet leptons and new gauge boson*, *Nucl. Phys. B* **644** (2002) 290 [hep-ph/0206150] [INSPIRE].

[72] T. Hambye et al., *Constraints on neutrino masses from leptogenesis models*, *Nucl. Phys. B* **695** (2004) 169 [hep-ph/0312203] [INSPIRE].

[73] T. Fukuyama, H. Sugiyama and K. Tsumura, *Constraints from muon g − 2 and LFV processes in the Higgs triplet model*, *JHEP* **03** (2010) 044 [arXiv:0909.4943] [INSPIRE].

[74] R. Coy and M. Frigerio, *Effective approach to lepton observables: the seesaw case*, *Phys. Rev. D* **99** (2019) 095040 [arXiv:1812.03165] [INSPIRE].

[75] D. Wyler and L. Wolfenstein, *Massless neutrinos in left-right symmetric models*, *Nucl. Phys. B* **218** (1983) 205 [INSPIRE].

[76] R.N. Mohapatra and J.W.F. Valle, *Neutrino mass and baryon number nonconservation in superstring models*, *Phys. Rev. D* **34** (1986) 1642 [INSPIRE].

[77] M.C. Gonzalez-Garcia and J.W.F. Valle, *Fast decaying neutrinos and observable flavor violation in a new class of Majoron models*, *Phys. Lett. B* **216** (1989) 360 [INSPIRE].

[78] J. Kersten and A.Y. Smirnov, *Right-handed neutrinos at CERN LHC and the mechanism of neutrino mass generation*, *Phys. Rev. D* **76** (2007) 073005 [arXiv:0705.3221] [INSPIRE].

[79] Y. Cai et al., *From the trees to the forest: a review of radiative neutrino mass models*, *Front. in Phys.* **5** (2017) 63 [arXiv:1706.08524] [INSPIRE].

[80] K.S. Babu and J. Julio, *Two-loop neutrino mass generation through leptoquarks*, *Nucl. Phys. B* **841** (2010) 130 [arXiv:1006.1092] [INSPIRE].

[81] T. Nomura, H. Okada and Y. Orikasa, *SU(2)$_L$ septet scalar linking to a radiative neutrino model*, *Phys. Rev. D* **94** (2016) 055012 [arXiv:1605.02601] [INSPIRE].

[82] T. Nomura and H. Okada, *An extended colored Zee-Babu model*, *Phys. Rev. D* **94** (2016) 075021 [arXiv:1607.04952] [INSPIRE].

[83] S.J. Lee, T. Nomura and H. Okada, *Radiatively induced neutrino mass model with flavor dependent gauge symmetry*, *Nucl. Phys. B* **931** (2018) 179 [arXiv:1702.03733] [INSPIRE].

[84] C.-W. Chiang, H. Okada and E. Senaha, *Dark matter, muon g − 2, electric dipole moments, and Z → ℓ$_i^+$ℓ$_j^-$ in a one-loop induced neutrino model*, *Phys. Rev. D* **96** (2017) 015002 [arXiv:1703.09153] [INSPIRE].

[85] S. Saad, *Combined explanations of (g − 2)$_\mu$, R$_{D^{(*)}}$, R$_{K^{(*)}}$ anomalies in a two-loop radiative neutrino mass model*, *Phys. Rev. D* **102** (2020) 015019 [arXiv:2005.04352] [INSPIRE].

[86] S. Jana, P.K. Vishnu, W. Rodejohann and S. Saad, *Dark matter assisted lepton anomalous magnetic moments and neutrino masses*, *Phys. Rev. D* **102** (2020) 075003 [arXiv:2008.02377] [INSPIRE].

[87] A. Alvarez et al., *Accommodating muon (g − 2) and leptogenesis in a scotogenic model*, *JHEP* **06** (2023) 163 [arXiv:2301.08485] [INSPIRE].

[88] R.K. Barman, R. Dcruz and A. Thapa, *Neutrino masses and magnetic moments of electron and muon in the Zee model*, *JHEP* **03** (2022) 183 [arXiv:2112.04523] [INSPIRE].

[89] D.A. Dicus, H.-J. He and J.N. Ng, *Neutrino-lepton masses, Zee scalars and muon g − 2*, *Phys. Rev. Lett.* **87** (2001) 111803 [hep-ph/0103126] [INSPIRE].

[90] E. Ma, *Naturally small seesaw neutrino mass with no new physics beyond the TeV scale*, *Phys. Rev. Lett.* **86** (2001) 2502 [hep-ph/0011121] [INSPIRE].

[91] E. Ma and M. Raidal, *Neutrino mass, muon anomalous magnetic moment, and lepton flavor nonconservation*, *Phys. Rev. Lett.* **87** (2001) 011802 [*Erratum ibid.* **87** (2001) 159901] [hep-ph/0102255] [INSPIRE].

[92] S. Gabriel and S. Nandi, *A new two Higgs doublet model*, *Phys. Lett. B* **655** (2007) 141 [hep-ph/0610253] [INSPIRE].

[93] F. Wang, W. Wang and J.M. Yang, *Split two-Higgs-doublet model and neutrino condensation*, *EPL* **76** (2006) 388 [hep-ph/0601018] [INSPIRE].

[94] S.M. Davidson and H.E. Logan, *Dirac neutrinos from a second Higgs doublet*, *Phys. Rev. D* **80** (2009) 095008 [arXiv:0906.3335] [INSPIRE].

[95] S. Kanemura, T. Matsui and H. Sugiyama, *Loop suppression of Dirac neutrino mass in the neutrinophilic two Higgs doublet model*, *Phys. Lett. B* **727** (2013) 151 [arXiv:1305.4521] [INSPIRE].

[96] P.A.N. Machado et al., *On the viability of minimal neutrinophilic two-Higgs-doublet models*, *JHEP* **12** (2015) 160 [arXiv:1507.07550] [INSPIRE].

[97] N. Haba and K. Tsumura, *ν-two Higgs doublet model and its collider phenomenology*, *JHEP* **06** (2011) 068 [arXiv:1105.1409] [INSPIRE].

[98] N. Haba and M. Hirotsu, *TeV-scale seesaw from a multi-Higgs model*, *Eur. Phys. J. C* **69** (2010) 481 [arXiv:1005.1372] [INSPIRE].

[99] N. Haba, T. Omija and T. Yamada, *Charged lepton flavor violating processes in neutrinophilic Higgs + seesaw model*, *PTEP* **2020** (2020) 073B08 [arXiv:2004.01896] [INSPIRE].

[100] B. Fu and S.F. King, *Leptogenesis in type Ib seesaw models*, *Phys. Rev. D* **105** (2022) 095001 [arXiv:2107.01486] [INSPIRE].

[101] J. Hernandez-Garcia and S.F. King, *New Weinberg operator for neutrino mass and its seesaw origin*, *JHEP* **05** (2019) 169 [arXiv:1903.01474] [INSPIRE].

[102] P. Escribano, J. Terol-Calvo and A. Vicente, *$(g-2)_{e,\mu}$ in an extended inverse type-III seesaw model*, *Phys. Rev. D* **103** (2021) 115018 [arXiv:2104.03705] [INSPIRE].

[103] C.-H. Chen, C.-W. Chiang and T. Nomura, *Muon $g-2$ in a two-Higgs-doublet model with a type-II seesaw mechanism*, *Phys. Rev. D* **104** (2021) 055011 [arXiv:2104.03275] [INSPIRE].

[104] A.E.C. Hernández, S.F. King and H. Lee, *Fermion mass hierarchies from vectorlike families with an extended 2HDM and a possible explanation for the electron and muon anomalous magnetic moments*, *Phys. Rev. D* **103** (2021) 115024 [arXiv:2101.05819] [INSPIRE].

[105] A. de Giorgi, L. Merlo and S. Pokorski, *The low-scale seesaw solution to the M_W and $(g-2)_\mu$ anomalies*, *Fortsch. Phys.* **71** (2023) 2300020 [arXiv:2211.03797] [INSPIRE].

[106] T. Mondal and H. Okada, *Inverse seesaw and $(g-2)$ anomalies in B-L extended two Higgs doublet model*, *Nucl. Phys. B* **976** (2022) 115716 [arXiv:2103.13149] [INSPIRE].

[107] A. Zee, *A theory of lepton number violation, neutrino Majorana mass, and oscillation*, *Phys. Lett. B* **93** (1980) 389 [*Erratum ibid.* **95** (1980) 461] [INSPIRE].

[108] ALEPH et al. collaborations, *Search for charged Higgs bosons: combined results using LEP data*, *Eur. Phys. J. C* **73** (2013) 2463 [arXiv:1301.6065] [INSPIRE].

[109] PARTICLE DATA GROUP collaboration, *Review of particle physics*, *PTEP* **2020** (2020) 083C01 [INSPIRE].

[110] MU3E collaboration, *The Mu3e data acquisition*, *IEEE Trans. Nucl. Sci.* **68** (2021) 1833 [arXiv:2010.15648] [INSPIRE].

[111] HFLAV collaboration, *Averages of b-hadron, c-hadron, and τ-lepton properties as of* 2018, *Eur. Phys. J. C* **81** (2021) 226 [`arXiv:1909.12524`] [InSPIRE].

[112] BELLE-II collaboration, *The Belle II physics book*, *PTEP* **2019** (2019) 123C01 [*Erratum ibid.* **2020** (2020) 029201] [`arXiv:1808.10567`] [InSPIRE].

[113] MEG II collaboration, *The design of the MEG II experiment*, *Eur. Phys. J. C* **78** (2018) 380 [`arXiv:1801.04688`] [InSPIRE].

[114] SINDRUM II collaboration, *A search for muon to electron conversion in muonic gold*, *Eur. Phys. J. C* **47** (2006) 337 [InSPIRE].

[115] MU2E collaboration, *Muon to electron conversion search in the presence of Al nuclei at the Fermilab Mu2e experiment: motivation, design and progress*, *PoS* **ICHEP2020** (2021) 439 [InSPIRE].

[116] MU2E collaboration, *Mu2e conceptual design report*, `arXiv:1211.7019` [InSPIRE].

[117] COMET collaboration, *The COherent Muon to Electron Transition (COMET) experiment*, *Nucl. Phys. B Proc. Suppl.* **218** (2011) 38 [InSPIRE].

[118] COMET collaboration, *COMET phase-I technical design report*, *PTEP* **2020** (2020) 033C01 [`arXiv:1812.09018`] [InSPIRE].

[119] COMET and MU2E collaborations, *Experimental searches for muon to electron conversion in a nucleus: COMET, DeeMe, and Mu2e. A contributed paper for Snowmass 21*, in the proceedings of the *Snowmass* 2021, (2022) [`arXiv:2203.07089`] [InSPIRE].

[120] R.J. Barlow, *The PRISM/PRIME project*, *Nucl. Phys. B Proc. Suppl.* **218** (2011) 44 [InSPIRE].

[121] Y. Kuno and Y. Okada, *Muon decay and physics beyond the Standard Model*, *Rev. Mod. Phys.* **73** (2001) 151 [`hep-ph/9909265`] [InSPIRE].

[122] S. Weinberg and G. Feinberg, *Electromagnetic transitions between μ meson and electron*, *Phys. Rev. Lett.* **3** (1959) 111 [InSPIRE].

[123] V. Cirigliano, R. Kitano, Y. Okada and P. Tuzon, *On the model discriminating power of μ → e conversion in nuclei*, *Phys. Rev. D* **80** (2009) 013002 [`arXiv:0904.0957`] [InSPIRE].

[124] E. Bertuzzo, Y.F. Perez G., O. Sumensari and R. Zukanovich Funchal, *Limits on neutrinophilic two-Higgs-doublet models from flavor physics*, *JHEP* **01** (2016) 018 [`arXiv:1510.04284`] [InSPIRE].

[125] E. Arganda, M.J. Herrero and A.M. Teixeira, *μ-e conversion in nuclei within the CMSSM seesaw: universality versus non-universality*, *JHEP* **10** (2007) 104 [`arXiv:0707.2955`] [InSPIRE].

[126] R. Kitano, M. Koike and Y. Okada, *Detailed calculation of lepton flavor violating muon electron conversion rate for various nuclei*, *Phys. Rev. D* **66** (2002) 096002 [*Erratum ibid.* **76** (2007) 059902] [`hep-ph/0203110`] [InSPIRE].

[127] F. Feruglio and A. Romanino, *Lepton flavor symmetries*, *Rev. Mod. Phys.* **93** (2021) 015007 [`arXiv:1912.06028`] [InSPIRE].

[128] ACME collaboration, *Order of magnitude smaller limit on the electric dipole moment of the electron*, *Science* **343** (2014) 269 [`arXiv:1310.7534`] [InSPIRE].

[129] ACME collaboration, *Improved limit on the electric dipole moment of the electron*, *Nature* **562** (2018) 355 [InSPIRE].

[130] Muon (g-2) collaboration, *An improved limit on the muon electric dipole moment*, [*Phys. Rev. D* **80** (2009) 052008](arXiv:0811.1207) [ɪɴSPIRE].

[131] P.F. de Salas et al., *Status of neutrino oscillations* 2018*: 3σ hint for normal mass ordering and improved CP sensitivity*, [*Phys. Lett. B* **782** (2018) 633](arXiv:1708.01186) [ɪɴSPIRE].

[132] S.S.D. Willenbrock, *Pair production of supersymmetric charged Higgs bosons*, [*Phys. Rev. D* **35** (1987) 173](ɪɴSPIRE).

[133] O. Brein and W. Hollik, *Pair production of charged MSSM Higgs bosons by gluon fusion*, [*Eur. Phys. J. C* **13** (2000) 175](hep-ph/9908529) [ɪɴSPIRE].

[134] F.F. Deppisch, P.S. Bhupal Dev and A. Pilaftsis, *Neutrinos and collider physics*, [*New J. Phys.* **17** (2015) 075019](arXiv:1502.06541) [ɪɴSPIRE].

[135] M.S. Bilenky and A. Santamaria, *One loop effective Lagrangian for a Standard Model with a heavy charged scalar singlet*, [*Nucl. Phys. B* **420** (1994) 47](hep-ph/9310302) [ɪɴSPIRE].

[136] M. Raidal and A. Santamaria, *Muon electron conversion in nuclei versus μ → eγ: an effective field theory point of view*, [*Phys. Lett. B* **421** (1998) 250](hep-ph/9710389) [ɪɴSPIRE].